

Vibrational Assignment of Torsional Normal Modes of Rhodopsin: Probing Excited-State Isomerization Dynamics along the Reactive C₁₁=C₁₂ Torsion Coordinate

Steven W. Lin,^{†,‡} Michel Groesbeek,^{§,||} Ineke van der Hoef,[§] Peter Verdegem,[§] Johan Lugtenburg,[§] and Richard A. Mathies^{*,†}

Department of Chemistry, University of California, Berkeley, California 94720, and Leiden Institute of Chemistry, Leiden University, 2300 RA Leiden, The Netherlands

Received: August 22, 1997; In Final Form: November 25, 1997

The resonance Raman spectrum of the 11-*cis* retinal protonated Schiff base chromophore in rhodopsin exhibits low-frequency normal modes at 93, 131, 246, 260, 320, 446, and 568 cm⁻¹. Their relatively strong Raman activities reveal that the photoexcited chromophore undergoes rapid nuclear motion along torsional coordinates that may be involved in the 200-fs isomerization about the C₁₁=C₁₂ bond. Resonance Raman spectra of rhodopsins regenerated with isotopically labeled retinal derivatives and demethyl retinal analogues were obtained in order to determine the vibrational character of these low-frequency modes and to assign the C₁₁=C₁₂ torsional mode. ¹³C substitutions of atoms in the C₁₂–C₁₃ or C₁₃=C₁₄ bond cause the 568-cm⁻¹ mode to shift by ~8 cm⁻¹, and deuteration of the C₁₁=C₁₂ bond downshifts the 568- and 260-cm⁻¹ modes by ~35 and 5 cm⁻¹, respectively. The magnitudes of these shifts are consistent with those calculated for modes containing significant C₁₁=C₁₂ torsional character. Thus, we assign the 568-cm⁻¹ mode to a localized C₁₁=C₁₂ torsion and the 260-cm⁻¹ mode to a more delocalized torsional vibration involving coordinates from C₁₀ to C₁₃. Consistent with these assignments, these two modes are not Raman active in 13-demethyl, 11-*cis* rhodopsin which has a planar C₁₀...C₁₃ geometry. Furthermore, the relative Raman scattering strengths of the 260- and 568-cm⁻¹ modes are ~2-fold higher with preresonant excitation. These data quantitate the instantaneous torsional dynamics of the chromophore about its C₁₁=C₁₂ bond on the S₁ surface and indicate that the isomerization process is facilitated by vibronic coupling of the S₁ and S₂ surfaces via C₁₁=C₁₂ torsional distortion, which reduces the excited-state barrier along the reaction trajectory. We have also examined the low-frequency Raman spectrum of the *trans* primary photoproduct, bathorhodopsin, and discuss the relevance of its low-frequency torsional modes at ~54, 92, 128, 151, 262, 276, 324, and 376 cm⁻¹ to the observed femtosecond photochemical dynamics.

Introduction

Photoreceptor cells in the retina contain the biochemical machinery that enables the detection of optical images. The visual transduction process begins when the pigment chromophore in rhodopsin absorbs a photon and photochemically converts the protein to its active metarhodopsin-II structure.¹ Meta-II then catalytically activates several signal transducing "G" proteins that act on effector molecules to cause the closure of ion channels, resulting in the hyperpolarization of the plasma membrane.² Three kinds of cone photoreceptor cells, each containing a distinct visual pigment with absorption maxima (λ_{max}) at ~420, 530, or 560 nm mediate color vision. Rod photoreceptor cells, used for night vision, contain the pigment rhodopsin which absorbs maximally at 498 nm. All visual pigments consist of a ~40-kD polypeptide domain and an 11-*cis* retinal chromophore that is covalently linked to a conserved lysine residue by a protonated Schiff base (PSB) bond. The

polypeptide is folded into seven α -helical transmembrane segments that form a well-defined steric and dielectric binding pocket for the chromophore. The pigments share some sequence identity, but specific differences in the composition of amino acids that line the chromophore binding pocket modulate the retinal transition energy and give rise to pigments with varying spectral sensitivities.

The primary photochemical reaction in vision is the light-induced *cis*-to-*trans* isomerization of the retinal chromophore about its C₁₁=C₁₂ bond to form a high-energy red-absorbing primary photoproduct called bathorhodopsin (Figure 1).¹ This reaction occurs with a temperature-independent quantum yield of ~0.67 and has been modeled theoretically to proceed along a barrierless trajectory on the S₁ surface.³ Early measurements of the formation time of the primary *trans* photoproduct indicated a time constant of <6 ps.^{4,5} Time-resolved resonance Raman spectroscopy⁶ detected the formation of a photoproduct within 30 ps, whose vibrational spectrum was similar to that of bathorhodopsin trapped at 77 K. Subsequent kinetic studies revealed that a red-shifted ground-state product designated photorhodopsin first forms in 20 ps and then relaxes to bathorhodopsin with a time constant of 40 ps.⁷ Furthermore, estimates of the excited-state lifetime from fluorescence quantum yield,^{8,9} resonance Raman intensity,^{10,11} and low-temperature hole-burning experiments¹² are consistent with the relaxation

* To whom correspondence should be addressed. E-mail address: rich@zinc.cchem.berkeley.edu.

[†] University of California.

[‡] Present address: Howard Hughes Medical Institute, Rockefeller University, 1230 York Ave., New York, NY 10021.

[§] Leiden University.

^{||} Present address: Department of Molecular Biophysics and Biochemistry, Yale University, 266 Whitney Ave., P.O. Box 208114, New Haven, CT 06511.

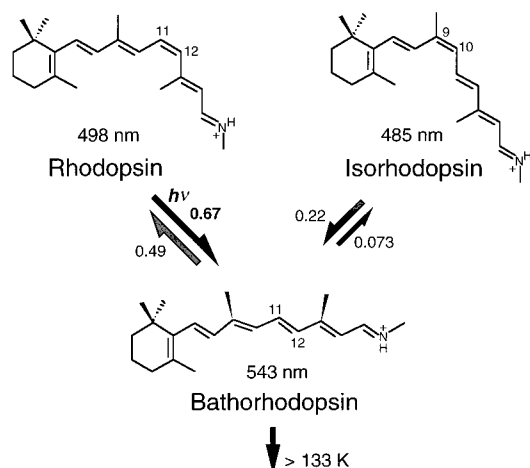


Figure 1. Photochemical conversion pathways between rhodopsin, isorhodopsin, and bathorhodopsin. The geometry of the retinal PSB chromophore is 11-*cis* in rhodopsin, 9-*cis* in isorhodopsin, and twisted all-*trans* in bathorhodopsin. The quantum yields of the photoisomerization reactions at 77 K³ and the absorption maxima of the pigments are indicated. The thermal decay of bathorhodopsin is inhibited below 133 K.

of the excited chromophore out of the S_1 Franck–Condon (FC) region in 100–500 fs, suggesting that the isomerization occurs on a sub-picosecond time scale.

The application of femtosecond lasers to this problem by the research groups of Shank and Mathies have enabled the direct observation of excited-state processes during the rhodopsin photoisomerization.^{13,14} These studies, using ~35-fs pump and 10-fs probe pulses to monitor absorption changes, have determined that a red-shifted ground-state photoproduct is completely formed in only 200 fs. Furthermore, the kinetic traces of the product signal display characteristic oscillations that suggest vibrationally coherent photoproduct production.¹⁵ This primary reaction is followed by a slow conformational relaxation of the *trans* chromophore and the protein moiety, which presumably corresponds to the photorhodopsin-to-bathorhodopsin transition. In comparison, the photoisomerization of the 11-*cis* retinal PSB to its all-*trans* isomer occurs with a quantum yield of ~0.2 in methanol^{16,17} and requires 10 ps for completion.^{16,18,19}

What are the molecular factors that drive the ultrafast isomerization of the 11-*cis* retinal PSB chromophore in condensed phase at room temperature? The femtosecond absorption studies indicate that the isomerization is complete before significant dephasing and relaxation of the excited vibrational wave packet has occurred. In addition, the photoproduct-formation time of 200 fs is on the order of the vibrational period of a typical torsional (~200-cm⁻¹) mode in polyenes.²⁰ These observations suggest that the ultrafast isomerization may be facilitated by the initial excited-state nuclear dynamics along the $C_{11}=C_{12}$ torsion normal coordinate, which direct the chromophore to distort along the correct trajectory toward the *trans* configuration. The origin of this facilitation has been suggested to be the geometric distortion of the $C_{11}=C_{12}$ region induced by the intramolecular steric interaction of the 10H atom with the 13-methyl group.^{13–15,21} The role of this steric interaction in the photochemistry has been investigated by examining the isomerization kinetics of the 9-*cis* retinal and 11-*cis*, 13-demethyl retinal chromophores in the pigments isorhodopsin and 13-demethyl rhodopsin, respectively.^{22,23} Femtosecond absorption measurements show that both chromophores, which lack intramolecular steric interactions involving the 13-methyl group, isomerize on a slower time scale (400–

600 fs). In addition, the isomerization quantum yields in these pigments are lower compared to that of rhodopsin, suggesting a causal relationship between the speed of the isomerization and its quantum efficiency.²¹ These observations taken together with the observed vibrational coherence of the isomerization in the native pigment suggest that the photochemistry of the 11-*cis* retinal chromophore in rhodopsin proceeds along a barrierless coordinate that couples the S_1 and S_0 surfaces via a dynamic photochemical internal conversion process.^{15,22}

To understand the dynamics and the mechanism of the isomerization process in rhodopsin, it is necessary to identify the normal modes of the 11-*cis* chromophore that project along the reaction coordinate and then to determine the atomic motions that make up the excited-state reaction trajectory. This information on the initial excited-state dynamics can be obtained through an analysis of resonance Raman (RR) spectra.^{24,25} The vibrational scattering intensities of normal modes that experience shifts in their equilibrium geometries upon electronic excitation are selectively enhanced in a RR spectrum, and their scattering strengths reflect the degree of distortion along these coordinates. The determination of the vibrational character of the RR-active normal modes and the analysis of their scattering intensities provide quantitative information about the types and the magnitude of nuclear motions that govern the photochemistry and photophysics. RR intensity analysis has been utilized to probe the excited-state dynamics associated with the isomerization of *cis*-stilbene, bacteriorhodopsin,²⁶ and rhodopsin,¹⁰ as well as pericyclic photochemical rearrangements.²⁷

The RR spectrum of rhodopsin^{28–30} exhibits a number of spectral features that may be photochemically relevant. A mode at 970 cm⁻¹, which corresponds to the coupled A_2 vibration of the *cis* hydrogens on the $C_{11}=C_{12}$ bond, displays unusually strong activity.³¹ The intensity of this hydrogen out-of-plane (HOOP) vibration indicates that the photoexcited molecule immediately distorts by twisting about the $C_{11}=C_{12}$ bond. Eyring et al.³¹ proposed that the isomerization first proceeds along this HOOP coordinate, with the 11H and 12H atoms moving out of the plane by 5–10°, and then relaxes along a yet-unidentified low-frequency (~200-cm⁻¹) skeletal torsional coordinate that is primarily responsible for carrying the reaction to completion. Later, in a more complete study of the rhodopsin RR fundamental modes between 50 and 1700 cm⁻¹, Loppnow and Mathies¹⁰ detected intense low-frequency bands at 98, 135, 249, 262, and 336 cm⁻¹ which potentially represented the torsional coordinate(s) directly relevant to the isomerization. A complete Franck–Condon analysis of the absorption spectrum and RR excitation profiles showed that these torsional modes make a significant contribution to the rapid femtosecond relaxation of the chromophore in the excited state. However, these studies were not able to specify which torsional coordinates were relevant to the isomerization mechanism because the vibrational character of the low-frequency modes was not known.

The vibrational character of the Raman-active modes of rhodopsin between 900 and 1700 cm⁻¹ have previously been analyzed.^{32,33} In the present study, we extend this analysis to the low-frequency region, using isotopically labeled retinal derivatives and normal mode analysis to determine the vibrational character of the Raman-active modes and, specifically, to assign the $C_{11}=C_{12}$ torsional normal mode. The low-frequency modes of isorhodopsin and demethyl rhodopsins and of model retinal PSB compounds are also characterized and used to support these assignments. The observed similarities and differences in the patterns of the low-frequency bands among

the pigments and the model compounds are correlated with the structures and the photochemical and/or photophysical properties of the retinal chromophores to determine the excited-state nuclear motions that are important for the efficient *cis*–*trans* isomerization of the 11-*cis* chromophore in rhodopsin. In addition, we have obtained the RR spectrum of the low-frequency region of bathorhodopsin, and this gives us the opportunity to discuss the significance of its low-frequency modes in relation to the structure of its all-*trans* chromophore and the vibrational coherence observed in the rhodopsin-to-bathorhodopsin reaction.¹⁵

Materials and Methods

Retinal Synthesis. The syntheses and characterization of the isotopically labeled retinal derivatives {10,11-di-¹³C, 12,13-di-¹³C, 13,14-di-¹³C,³⁴ and 11,12-dideutero³⁵} and the 9- and 13-demethyl retinal analogues³⁶ have been described by Lugtenburg and co-workers.

Preparation of Rhodopsin. Rod outer segments (ROS) were isolated from bovine retinas (J. A. Lawson, Lincoln, NE) by sucrose flotation and density gradient centrifugation.³³ ROS were lysed in distilled water and solubilized in Ammonyx-LO (10% (v/v)) detergent (Exciton, Dayton, OH). Rhodopsin was purified by hydroxylapatite (HA) column chromatography³⁷ and eluted in 100 mM phosphate buffer (pH 6.7) containing Ammonyx-LO (<1% (v/v)). A typical yield of purified rhodopsin was ~1 μ mol from 100 retinas ($\epsilon_{\text{max}} \sim 40\,600\text{ cm}^{-1}\text{ M}^{-1}$ at 498 nm). Isorhodopsin was prepared photochemically by irradiating a solution of purified rhodopsin frozen in liquid nitrogen with defocused 568.2-nm light (~70 mW/cm²)³⁸ from a Kr⁺ laser (Spectra Physics 2025-11) for ~30 min. The conversion of rhodopsin to isorhodopsin was assayed by the shift of the λ_{max} of the irradiated pigment solution from 498 to ~485 nm. The purity of this sample was subsequently assayed using resonance Raman spectroscopy. Its spectrum was consistent with the amount of isorhodopsin in the sample being greater than 95%.

Regeneration of Rhodopsin with Synthetic Retinals. Lysed ROS suspended in 100 mM phosphate buffer (pH 7) were bleached by ambient light at room temperature in the presence of 10 mM hydroxylamine (pH 7) and then washed three times in phosphate buffer. Bleached ROS resuspended in phosphate buffer were incubated at room temperature with one of the following retinals: 9-demethyl, 11-*cis* retinal; 13-demethyl, 11-*cis* retinal; 10,11-di-¹³C-, 12,13-di-¹³C-, or 13,14-di-¹³C-labeled 11-*cis* retinal; and 11,12-D₂, 11-*cis* retinal. Regenerated ROS were washed in phosphate buffer, solubilized in Ammonyx-LO, and purified by HA chromatography. If necessary, the purified pigment solution was concentrated by membrane filtration (Amicon Centriprep-30). The absorption maxima (λ_{max}) of rhodopsins regenerated with di-¹³C and 11,12-D₂ retinals were ~498 nm.

Resonance Raman Spectroscopy. Resonance Raman scattering was excited by focusing 488.0- or 514.5-nm light from an Ar⁺ laser (Spectra Physics 2020) with a 75-mm focal-length spherical lens (~20- μ m beam diameter) onto a solution of pigment (~12 μ M) flowing at ~900 cm/s through a glass capillary (0.08-cm diameter).^{28,32} The laser powers of ~0.5 and ~1.0 mW for the rhodopsin and isorhodopsin experiments, respectively, gave a value for the single-pass photoalteration that was less than 0.15. Solution from the sample reservoir (~12 mL on ice) was recirculated through the flow cell using a peristaltic pump.

Raman scattering was detected by a liquid-N₂-cooled CCD detector (Model LN-1152, Princeton Instruments) coupled to a

mismatched subtractive dispersion Spex 1400 double spectrograph.³⁹ Fluorescence background in the raw spectrum was removed by subtracting a spectrum of the bleached sample taken immediately after the pigment scan. Residual fluorescence was removed by subtracting a spline fit to the background. Spectra were corrected for the spectral sensitivity of the detection system using a standard quartz tungsten halogen lamp (EG&G, Model 590-20). The frequency axis was calibrated using Raman lines from CCl₄ and cyclohexane as standards. The resolution of the spectrum was ~6 cm⁻¹. Frequencies below 200 cm⁻¹ and between 200 and 1700 cm⁻¹ are accurate to ± 5 and ± 2 cm⁻¹, respectively.

Low-Temperature Resonance Raman Spectroscopy. A solution of purified rhodopsin was concentrated by filtration (Amicon CF25 centriflo or Centriprep-30) until its final maximal absorbance was ~10 OD (1-cm path length). The concentrated solution (~3 μ L) was diluted with glycerol (1:1 (v/v)) and pipetted into a glass capillary (0.08-cm diameter) which was placed inside a vacuum-jacketed glass cell.⁴⁰ The temperature in the cell (monitored by a thermocouple) was quickly lowered to ~90 K by circulating liquid-N₂-cooled N₂ gas, to convert the sample solution to a clear glass. Raman scattering was excited by a 488.0-nm probe beam (75-mm focal length) from an Ar⁺ laser, either in the presence or the absence of a coaxial 568.2-nm pump beam from the Kr⁺ laser. The lasers powers were 6 mW of 488.0-nm light in probe-only scans and ~1 mW of 488.0-nm and ~14 mW of 568-nm light in pump + probe scans. Raman scattering at 90° from the excitation beam was focused into the spectrograph and detected by the CCD detector. A spectrum of bleached rhodopsin (1:1 (v/v) dilution with glycerol) was used to subtract out most of the background fluorescence and glycerol solvent lines. Residual fluorescence was removed by subtracting a spline fit to the background. Spectra were corrected for spectral sensitivity and their frequencies calibrated as described above.

Preparation of *n*-Butylamine Protonated Schiff Bases. Retinal (1–3 μ mol of 11-*cis*, 9-*cis*, or 13-demethyl, 11-*cis*) dissolved in ~200 μ L of methanol (dehydrated with molecular sieves, ~3-Å diameter) was reacted with a 30-fold excess of the *n*-butylamine at room temperature for ~30 min to produce the *n*-butylamine retinal Schiff base ($\lambda_{\text{max}} \sim 360$ nm). The solvent containing unreacted *n*-butylamine was evaporated under a stream of N₂ gas, and the residue was redissolved in methanol (~150 μ L). The solution was titrated with aliquots of acidified methanol (~0.5 M HCl) until the Schiff base was protonated as judged by the shift of the λ_{max} to ~445 nm. Methanol titrated in the same way was prepared in parallel to serve as the blank.

Preresonance Raman Spectroscopy. Raman spectra of the retinal PSB's were obtained by exciting 100 μ L of solution in a glass capillary with 750-nm light (60 mW, 75-mm spherical focus) from a Ti:sapphire laser (Lexel 479) pumped by the all-lines output from an Ar⁺ laser. Scattering was detected by the CCD–spectrograph system equipped with gratings blazed at 750 nm. Due to the large dispersion (~0.38 Å/bin) across the detector face, a complete spectrum was generated by concatenating four overlapping ~600-cm⁻¹ wide windows. Solvent lines were removed by subtracting a spectrum of the blank solvent solution obtained immediately after the sample scan. CCl₄ and cyclohexane lines were used for frequency calibration. The resolution of these spectra was ~2 cm⁻¹, and frequencies are accurate to ± 3 cm⁻¹.

To obtain preresonance spectra of rhodopsin or isorhodopsin, ~50 μ L of concentrated pigment solution (~300 μ M) was pipetted into a square glass capillary (0.15 cm) and excited with

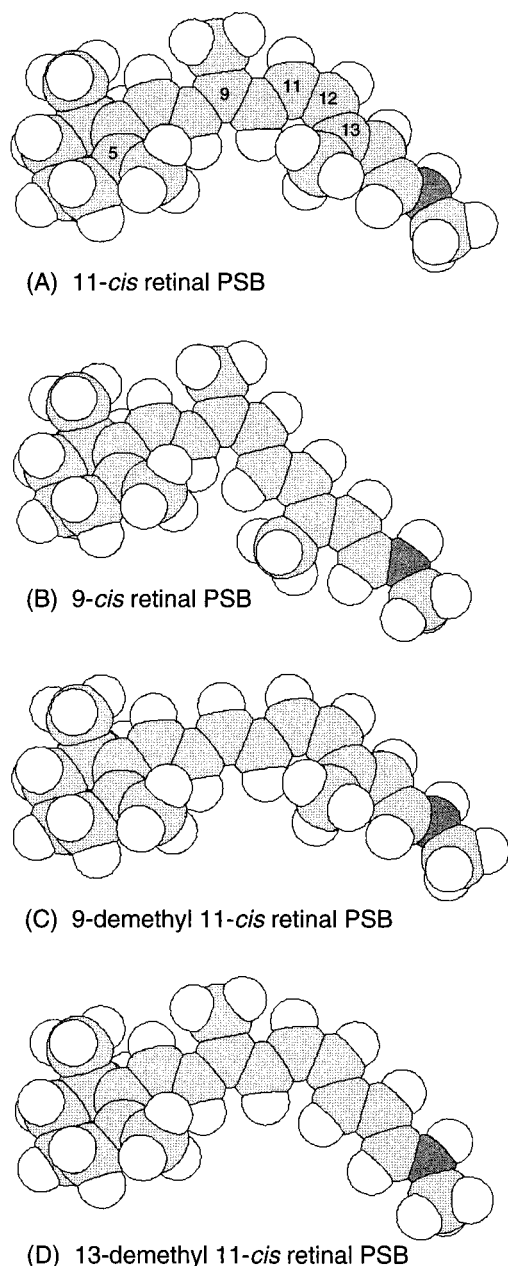


Figure 2. Minimum-energy structures of the retinal PSB molecules: (A) 11-*cis* PSB; (B) 9-*cis* PSB; (C) 9-demethyl, 11-*cis* PSB; (D) 13-demethyl, 11-*cis* PSB. White = hydrogen, light shade = carbon, dark shade = nitrogen.

792-nm light (100 mW, 75-mm spherical focus) from a Ti:sapphire laser. After the sample scan, the pigment was bleached using a 75-W incandescent lamp. A scan of this bleached solution was used for background subtraction. Five overlapping windows were concatenated to generate a spectrum covering 50–1700 cm^{-1} . CCl_4 and cyclohexane lines were used for frequency calibration. The resolution for these scans was $\sim 1.5 \text{ cm}^{-1}$. The accuracy of the frequencies is $\pm 5 \text{ cm}^{-1}$ below $\sim 200 \text{ cm}^{-1}$ and $\pm 3 \text{ cm}^{-1}$ between 200 and 1700 cm^{-1} . All spectra were corrected for detection sensitivity using a standard lamp.

Normal Mode Analysis. The normal modes of retinal PSB's were calculated using a modified version of the QCFF/PI program.²⁰ The retinal PSB molecule was terminated with a CH_2R group (R mass = 15 amu). Selected σ - and π -electron force-field parameters were adjusted to better reproduce the frequencies of the $\text{C}_7=\text{C}_8$ and $\text{C}_{11}=\text{C}_{12}$ HOOP vibrations of

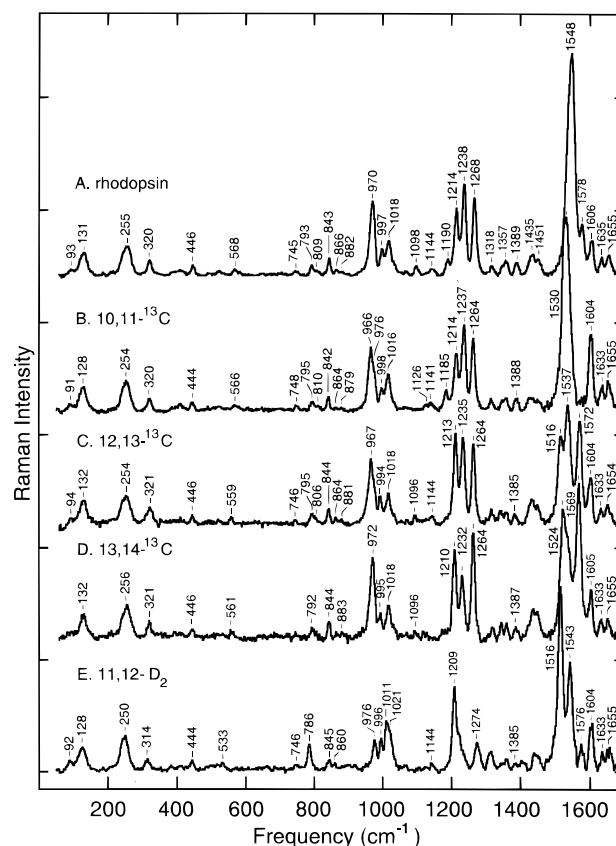


Figure 3. Resonance Raman spectrum of (A) rhodopsin regenerated with (B) 10,11-di- ^{13}C , (C) 12,13-di- ^{13}C , (D) 13,14-di- ^{13}C , and (E) 11,12- D_2 11-*cis* retinal. A flowing solution of purified rhodopsin was excited with 488-nm light from an Ar⁺ laser.

11-*cis* and 9-*cis* retinals and their PSB's. The modified parameters for the σ potential function involving sp^2 carbon (Cp) are as follows (notation as in ref 20): CpCp bond, $b_0 = 1.473 \text{ \AA}$, $D = 81.9 \text{ kcal mol}^{-1}$; CpC' bond, $b_0 = 1.404 \text{ \AA}$, $1/2K_b = 150 \text{ kcal mol}^{-1} \text{ \AA}^{-2}$, $D = 81.9 \text{ kcal mol}^{-1}$; XCpCpX torsion, $1/2K_\phi^{(2)} = 3.0 \text{ kcal mol}^{-1}$; HCpCPH torsion, $K_{\theta\theta'} = 0.3 \text{ kcal mol}^{-1} \text{ rad}^{-2}$. The value of β_0 in the Cp core resonance integral was set to -2.2385 eV . Parameters for the π -electron integrals of protonated Schiff base nitrogen were set to values listed in ref 41 except with $\beta_0 = -2.46 \text{ eV}$. Parameters for new σ -bond coordinates involving the Schiff base nitrogen and the R group are as follows: CpN , $b_0 = 1.394 \text{ \AA}$, $D = 130 \text{ kcal mol}^{-1}$, $\alpha = 1.7562 \text{ \AA}^{-1}$; CpR , $b_0 = 1.45 \text{ \AA}$, $1/2K_b = 250 \text{ kcal mol}^{-1} \text{ \AA}^{-2}$, $D = 88.0 \text{ kcal mol}^{-1}$; XCpNX torsion, $1/2K_\phi^{(2)} = 2.54 \text{ kcal mol}^{-1}$. The geometries of the 11-*cis* PSB, 9-*cis* PSB, 9-demethyl, 11-*cis* PSB, and 13-demethyl, 11-*cis* PSB were minimized without constraint (Figure 2). The normal modes were computed for the minimized structures.

Results

Resonance Raman (RR) spectra of the pigments studied here are presented first and correlated to modifications of the chromophore structure (Figure 2). Preresonance Raman spectra of model PSB compounds, rhodopsin, and isorhodopsin are then examined. These data are followed by a normal mode analysis of the low-frequency vibrations of the 11-*cis* PSB and its demethyl analogues.

Rhodopsin. Resonance Raman spectra of rhodopsin and its di- ^{13}C and 11,12-dideutero (D_2) derivatives are presented in Figure 3. Previous studies have focused on the assignments of

modes above 900 cm^{-1} .^{33,42} Our spectra of rhodopsin between 800 and 1700 cm^{-1} are in agreement with these data.

The 900–1700 cm^{-1} Region. The most intense mode is the in-phase C=C stretch at 1548 cm^{-1} . Other phase combinations of the individual C=C stretching coordinates appear with lower intensity at 1578, 1606, and 1635 cm^{-1} . The “fingerprint” modes between 1100 and 1270 cm^{-1} , comprised of C–C stretches, are sensitive to the chemical and geometric structure of retinal.⁴³ The $\text{C}_{10}\text{--C}_{11}$, $\text{C}_{14}\text{--C}_{15}$, $\text{C}_8\text{--C}_9$, and $\text{C}_{12}\text{--C}_{13}$ stretches of rhodopsin have been assigned at 1098, 1190, 1214, and 1238 cm^{-1} , respectively.³³ The vibrational pattern of the ^{13}C derivative spectra are consistent with these assignments. A mode at 1098 cm^{-1} is absent in 10,11- ^{13}C rhodopsin because the $\text{C}_{10}\text{--C}_{11}$ stretch has moved to lower frequency with reduced intensity. Substitutions made at the $\text{C}_{12}\text{--C}_{13}$ and $\text{C}_{13}\text{=C}_{14}$ bonds shift all of the fingerprint lines down by $\sim 3\text{--}5\text{ cm}^{-1}$ because the $\text{C}_{12}\text{--C}_{13}$ stretch character is mixed into all of the fingerprint modes.³³ The prominent band at 1268 cm^{-1} is the $\text{C}_{11}\text{=C}_{12}$ A_1 hydrogen rock that is characteristic of the 11-*cis* isomer.^{33,43} It is only slightly affected by ^{13}C substitution but downshifts dramatically upon 11,12- D_2 substitution (Figure 3E).

The $\text{C}_{11}\text{=C}_{12}$ A_2 HOOP mode at 970 cm^{-1} corresponds to the out-of-phase combination of the 11H and 12H wags.³¹ Dideutero substitution at this bond shifts this HOOP intensity down to 786 cm^{-1} . This shift also exposes a previously unresolved smaller peak at 976 cm^{-1} which can also be seen as a shoulder in the 10,11-di- ^{13}C data. Eyring et al.³¹ have assigned this band to the $\text{C}_7\text{=C}_8$ A_u HOOP vibration.

The 600–900 cm^{-1} Region. There are distinct bands at 843 and 793 cm^{-1} and smaller peaks at 882, 866, 809, and 745 cm^{-1} . Vibrational assignments for these modes may be suggested from comparisons with the normal modes of 11-*cis* and the all-*trans* retinals.^{42,43} On the basis of mode assignments in 11-*cis* retinal, the rhodopsin modes at 882 and 843 cm^{-1} may be assigned to the “–” and “+” combinations, respectively, of 10H and $\text{C}_7\text{=C}_8$ Bg HOOP wags and the 866 cm^{-1} mode to the 14H wag. Consistent with this, the 882 cm^{-1} band is downshifted 3 cm^{-1} in 10,11- ^{13}C rhodopsin. In contrast, there is almost no shift of the 843 cm^{-1} band, presumably because the “+” combination contains relatively weaker 10H wag character. This band does disappear when a deuterium is placed at C_{10} .³¹

The frequency of the symmetric C–C stretching mode of the ionone ring is at 792 cm^{-1} in all retinal isomers (9-*cis*, 11-*cis*, 13-*cis*, and all-*trans*) and in β -ionone and is insensitive to isotopic substitutions in the polyene moiety.^{29,43} A mode analogous to one at 793 cm^{-1} in the rhodopsin spectrum is also present in the spectra of pigments containing the 9-*cis* (isorhodopsin) and all-*trans* (bathorhodopsin) PSB chromophore.³³ In addition, this 793 cm^{-1} mode is shifted very little by isotopic substitutions. It is not visible in the 11,12- D_2 rhodopsin spectrum, presumably because it is masked by the downshifted $\text{C}_{11}\text{=C}_{12}$ A_2 HOOP mode at 786 cm^{-1} . Given their similar vibrational characteristics, the 793 cm^{-1} mode of rhodopsin is assigned to a C–C stretching vibration of the ionone ring. The mode at 745 cm^{-1} is also ascribed to a ring vibration because, like the 793 cm^{-1} mode, analogous bands are detected in both isorhodopsin and bathorhodopsin spectra.

The 50–600 cm^{-1} Region. The most interesting feature of the rhodopsin RR spectrum is the extensive series of low-frequency modes below 600 cm^{-1} which exhibit strong scattering intensity (Figure 4). The frequencies and the pattern of the observed modes are in good agreement with those first reported by Loppnow and Mathies.¹⁰ Most prominent are the

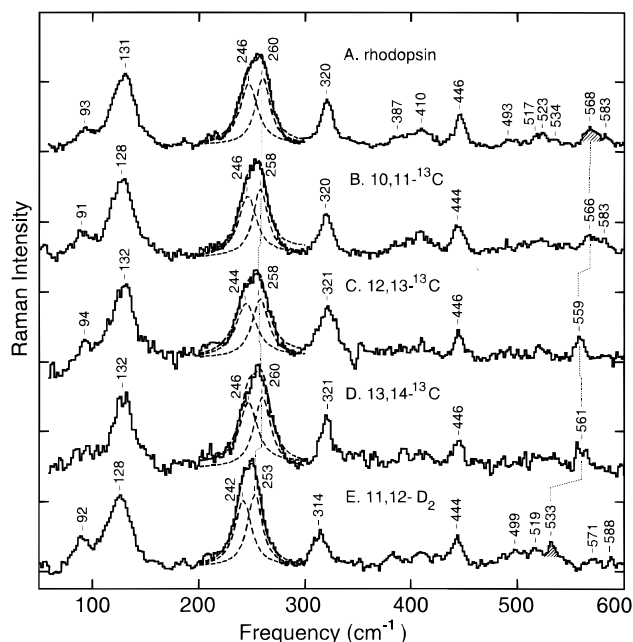


Figure 4. Expanded view of the 50–600- cm^{-1} region of the resonance Raman spectra from Figure 2: (A) rhodopsin and rhodopsin regenerated with (B) 10,11-di- ^{13}C , (C) 12,13-di- ^{13}C , (D) 13,14-di- ^{13}C , and (E) 11,12- D_2 11-*cis* retinal. The Lorentzian fit to the band at 255 cm^{-1} is indicated by the dashed lines.

modes at 131 and $\sim 255\text{ cm}^{-1}$. The large width and the asymmetrical shape of the band at 255 cm^{-1} suggest that it is a composite of two or more lines. This is more apparent in the spectrum of 11,12- D_2 rhodopsin in which the bandwidth of this line becomes narrower because the shoulder at $\sim 260\text{ cm}^{-1}$ has apparently shifted down by several wavenumbers. As shown in Figure 4, the profile of the 255 cm^{-1} band can be fit with two bands centered at 246 and 260 cm^{-1} which have similar RR intensities and bandwidths. These peaks are quite insensitive to ^{13}C substitutions, shifting by $\leq 2\text{ cm}^{-1}$. In contrast, dideutero substitution causes the original rhodopsin bands at 246 and 260 cm^{-1} to shift down by 4 and 7 cm^{-1} , respectively, as summarized in Figure 5A. The line at 131 cm^{-1} is less sensitive to the isotopic substitutions, but it is downshifted $\sim 3\text{ cm}^{-1}$ in 10,11-di- ^{13}C and 11,12- D_2 rhodopsin spectra.

Several bands with weaker intensity are detected at 93, 320, 446, and 568 cm^{-1} . The line at 568 cm^{-1} is the most interesting because its frequency is perturbed in all of the derivative spectra. It moves down by $\sim 8\text{ cm}^{-1}$ when the carbons on the $\text{C}_{12}\text{--C}_{13}$ or $\text{C}_{13}\text{=C}_{14}$ bond are labeled with ^{13}C and by 2 cm^{-1} when the $\text{C}_{10}\text{--C}_{11}$ bond is labeled. These shifts indicate that this mode involves vibration of the skeletal chain between C_{11} and C_{14} . Furthermore, the 11,12- D_2 substitution results in a loss of the intensity at 568 cm^{-1} . The position and the approximate size of features between 490 and 525 cm^{-1} appear relatively unchanged in the spectrum of the deuterated chromophore, but there is an increase in the intensity at 533 cm^{-1} . Similarly in the 11-*cis* PSB spectrum, the mode at 569 cm^{-1} moves down to $\sim 530\text{ cm}^{-1}$ in the 11,12- D_2 derivative (vide infra). On the basis of these observations, the band at 533 cm^{-1} in 11,12- D_2 rhodopsin is assigned to the shifted 568 cm^{-1} band. The large $\sim 35\text{ cm}^{-1}$ downshift indicates that the 568 cm^{-1} mode contains torsional and HOOP vibrational character of the $\text{C}_{11}\text{=C}_{12}$ bond. The 11,12-deuterations also shift the line originally at 320 cm^{-1} down by 6 cm^{-1} . On the other hand, the other lines are generally insensitive to the isotopic substitutions and their frequencies are within $\pm 2\text{ cm}^{-1}$ in all the derivative spectra. In

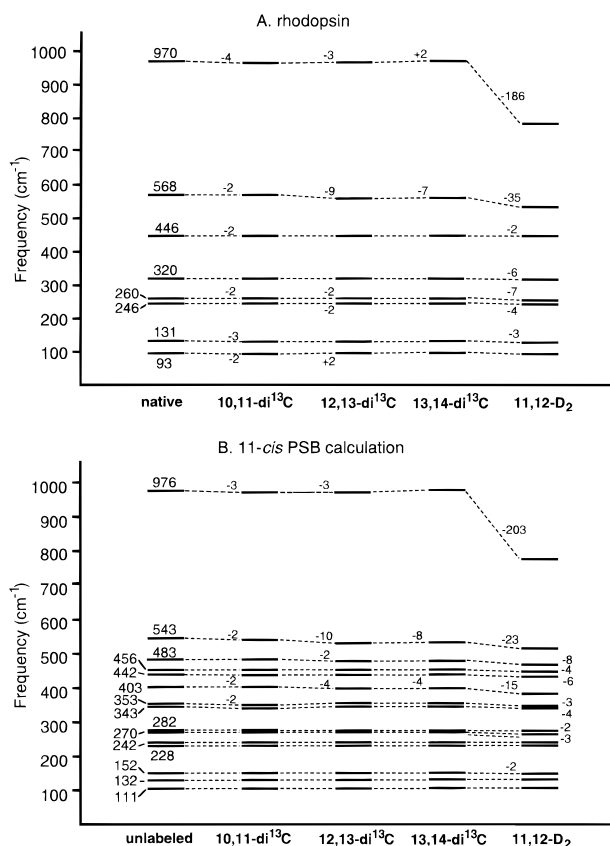


Figure 5. (A) Correlation diagram of low-frequency mode frequencies observed in rhodopsin and in pigments regenerated with isotopically labeled 11-*cis* retinal derivatives. (B) Theoretical correlation diagram of low-frequency modes of the 11-*cis* PSB and its isotopically labeled derivatives computed using the QCFF/PI method. Frequency shifts greater than 2 cm⁻¹ are enumerated.

13,14-di-¹³C rhodopsin, the line expected near 93 cm⁻¹ is not visible, most likely because of the higher background noise in this spectrum. Finally, a set of weaker bands are detected at 387, 410, 493, and 523 cm⁻¹.

Isorhodopsin. The 600–1700 cm⁻¹ Region. The vibrational characters of the normal modes of the 9-*cis* PSB chromophore in isorhodopsin, observed between 900 and 1700 cm⁻¹ (Figure 6), have been analyzed in detail.³³ The C₁₀–C₁₁ and C₁₂–C₁₃ stretching modes are located at 1151 and 1240 cm⁻¹, respectively, and the C₈–C₉ and C₁₄–C₁₅ stretches are degenerate at ~1204 cm⁻¹. The intense band at 959 cm⁻¹ has been assigned to the C₇=C₈ A_u HOOP vibration because it is insensitive to deuterium substitutions at C₁₀ or C₁₅ or at the C₁₁=C₁₂ bond.³¹ Bands with weaker intensity are also visible at 900, 882, 829, 794, 741, and 628 cm⁻¹. The lines at 741 and 794 cm⁻¹ are found with similar frequency and relative intensity as in rhodopsin.

The 50–600 cm⁻¹ Region. Like rhodopsin, several low-frequency modes of isorhodopsin display reasonably strong RR intensity (Figure 7). The frequencies and relative intensities of isorhodopsin bands at 93, 136, and 315 cm⁻¹ are very similar to those of rhodopsin lines at 93, 131, and 320 cm⁻¹. The lines at 242 and 351 cm⁻¹ with lower intensity appear to be unique to this isomer. Several overlapping bands can also be seen between 350 and 600 cm⁻¹.

¹³C substitution at the C₁₀–C₁₁, C₁₂–C₁₃, or C₁₃=C₁₄ bond has no effect on the position of the low-frequency bands within the resolution of the spectra (data not shown). However, 11,12-D₂ substitution shifts the 242-cm⁻¹ band down by 10 cm⁻¹ and

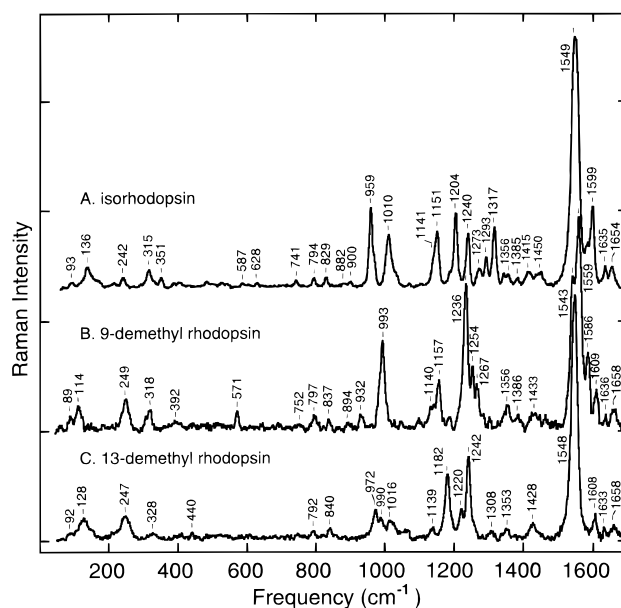


Figure 6. Resonance Raman spectrum of (A) isorhodopsin, (B) 9-demethyl rhodopsin, and (C) 13-demethyl rhodopsin. A flowing solution of purified pigment was excited with 488-nm light from an Ar⁺ laser.

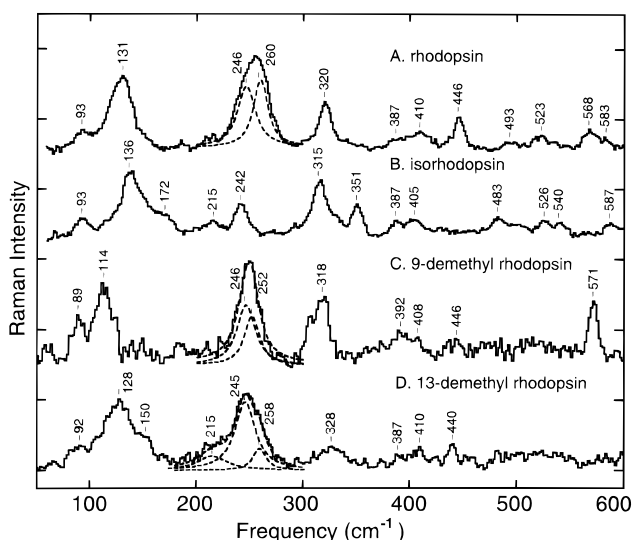


Figure 7. Expanded view of the 50–600-cm⁻¹ region of resonance Raman spectra from Figure 6: (A) rhodopsin; (B) isorhodopsin; (C) 9-demethyl rhodopsin; (D) 13-demethyl rhodopsin. The Lorentzian fit to the band at ~250 cm⁻¹ is indicated by the dashed lines.

results in ~15% reduction of the ~315 cm⁻¹ band intensity (data not shown). Smaller peaks originally at 540, 587, and 627 cm⁻¹ are not detected in the 11,12-D₂ data, apparently because they have moved down in frequency.

9-Demethyl Rhodopsin. 9-Demethyl, 11-*cis* retinal regenerates opsin with approximately 70% yield to produce a blue-shifted pigment with a λ_{max} at 465 nm. This value is in agreement with earlier measurements by Blatz and co-workers.^{44,45}

The 700–1700 cm⁻¹ Region. In the RR spectrum of 9-demethyl rhodopsin (Figure 6), there are two ethylenic lines at 1543 and 1559 cm⁻¹. The line at higher frequency is correlated with its blue-shifted λ_{max} ⁴⁶ and, thus, is assigned to the in-phase ethylenic stretch. The mode at 1543 cm⁻¹ is another ethylenic stretching vibration that has picked up RR intensity as a result of the structural modification. The C=NH

stretch at 1658 cm^{-1} is shifted up $\sim 4\text{ cm}^{-1}$ from its position in rhodopsin. The higher frequency may reflect the stronger interaction of the PSB group with its protein environment (accounting for the blue shift of the absorption band) or, alternatively, may be explained by increased kinetic coupling of the C=N stretch coordinate with the upshifted in-phase C=C stretch (although this latter effect is expected to be weak in retinals).⁴⁷

The fingerprint region of the 9-demethyl PSB chromophore is consistent with the changes expected when a chain methyl is removed. Vibrational assignments of these bands are facilitated by the normal mode analysis on all-*trans* retinal and its 9-demethyl analogue by Curry.⁴⁸ In all-*trans* retinal, the $\text{C}_{14}\text{--C}_{15}$, $\text{C}_{10}\text{--C}_{11}$, $\text{C}_8\text{--C}_9$, and $\text{C}_{12}\text{--C}_{13}$ stretches are located at 1111, 1163, 1197, and 1215 cm^{-1} , respectively.⁴³ The absence of the C_9 -methyl stretch coordinate in 9-demethyl all-*trans* retinal lowers the $\text{C}_8\text{--C}_9$ stretch closer to its intrinsic frequency so that it couples with the nearby $\text{C}_{10}\text{--C}_{11}$ stretch to form two modes at ~ 1145 and $\sim 1170\text{ cm}^{-1}$. The frequency of the $\text{C}_{12}\text{--C}_{13}$ stretch which is not kinetically coupled to the C_9 -methyl stretch in all-*trans* retinal remains at 1214 cm^{-1} in the 9-demethyl analogue. By analogy to these changes, the new line at 1157 cm^{-1} in 9-demethyl rhodopsin is assigned to the downshifted $\text{C}_8\text{--C}_9$ stretch, and the $\text{C}_{12}\text{--C}_{13}$ stretch is assigned at 1236 cm^{-1} . The absence of the 9-methyl group also allows the hydrogen wagging vibrations between C_7 and C_{12} to mix more effectively to form an in-phase HOOP combination at $\sim 1000\text{ cm}^{-1}$ in 9-demethyl all-*trans* retinal. This band should be conspicuous because a relatively strong band nearby at 1018 cm^{-1} in rhodopsin, which is due to the 9-methyl rock,⁴³ would be absent in 9-demethyl rhodopsin. Therefore, the intense line at 993 cm^{-1} is assigned to the coupled vibration of hydrogen wags between C_7 and C_{12} .

The RR spectrum of 9-demethyl rhodopsin is consistent with the FTIR difference spectrum of 9-demethyl rhodopsin.⁴⁹ The comparison is made with the (meta-I)–rhodopsin difference because the negative rhodopsin lines are more resolved from the positive photoproduct lines in this difference spectrum. The fingerprint region in the FTIR spectrum also exhibits lines at ~ 1150 and 1236 cm^{-1} . In addition, there is a strong band at 999 cm^{-1} that corresponds to the 993 cm^{-1} line in the RR data. The FTIR band at $\sim 1187\text{ cm}^{-1}$, which is absent in the RR spectrum, most likely represents the $\text{C}_{14}\text{--C}_{15}$ stretch because this mode is expected to have strong IR but weak RR intensity in retinal PSB's on the basis of the comparison of the FTIR^{50,51} and RR³³ spectra of rhodopsin and isorhodopsin.

The 50–600 cm^{-1} Region. The low-frequency region of 9-demethyl rhodopsin is qualitatively similar to that of rhodopsin. There are two strong lines at 114 and 249 cm^{-1} which are flanked by weaker lines at 89, 318, and 571 cm^{-1} (Figure 7). Assuming direct correspondence between the low-frequency bands of the two pigments, we find that the 131 cm^{-1} line in rhodopsin has moved down to 115 cm^{-1} and that the 568 cm^{-1} line has gained intensity and shifted up 3 cm^{-1} in the 9-demethyl pigment. The band at 249 cm^{-1} correlates to the broad rhodopsin band at 255 cm^{-1} . The width of this band is smaller in the 9-demethyl pigment, and it can be fit equally well with a single line centered at 249 cm^{-1} or with two peaks at 246 and 252 cm^{-1} . The former fit would imply that the position of one of the two lines at 246 and 260 cm^{-1} in rhodopsin has moved, while the other line has lost all of its intensity. The fit using two bands would imply that the 260 cm^{-1} band in rhodopsin moves down to 252 cm^{-1} and loses about half of its original intensity.

13-Demethyl Rhodopsin. The 13-demethyl rhodopsin pigment has a λ_{max} at 500 nm, consistent with previous studies.^{44,52} 13-Demethyl, 11-*cis* retinal regenerates opsin in ROS membranes at a very slow rate and with a maximum yield of $<50\%$.

The 700–1700 cm^{-1} Region. The main C=C band is at the same frequency as in rhodopsin, consistent with the fact that both pigments have the same λ_{max} . However, the C=NH stretching frequency is higher in the 13-demethyl pigment, perhaps due to stronger hydrogen bonding of the Schiff base nitrogen with a water molecule.⁴⁷ The band shifts seen in the fingerprint region (Figure 6) resulting from the removal of the 13-methyl group are analogous to those seen in the 9-demethyl pigment because the $\text{C}_{12}\text{--C}_{13}$ and $\text{C}_8\text{--C}_9$ bonds are located at a geometrically equivalent position in relation to the methyl groups in the unmodified 11-*cis* PSB. The fingerprint assignments for 13-demethyl rhodopsin are also facilitated by previous vibrational analyses on all-*trans* retinal and its 13-demethyl analogue.⁴⁸ In 13-demethyl all-*trans* retinal, the downshifted $\text{C}_{12}\text{--C}_{13}$ stretch mixes with the other C–C coordinates, forming an in-phase combination at 1186 cm^{-1} with contributions from the $\text{C}_{10}\text{--C}_{11}$, $\text{C}_{12}\text{--C}_{13}$, and $\text{C}_{14}\text{--C}_{15}$ stretches and an out-of-phase combination of the $\text{C}_{10}\text{--C}_{11}$ and $\text{C}_{12}\text{--C}_{13}$ stretches at 1157 cm^{-1} . The localized $\text{C}_8\text{--C}_9$ stretch is shifted up $\sim 5\text{ cm}^{-1}$ to 1222 cm^{-1} from its frequency in all-*trans* retinal. By analogy, the mode at 1182 cm^{-1} in 13-demethyl rhodopsin is assigned to an in-phase C–C stretch with $\text{C}_{12}\text{--C}_{13}$ character. The $\text{C}_8\text{--C}_9$ stretch is assigned to the 1220 cm^{-1} line, close to its frequency in rhodopsin. By process of elimination, the strong band at 1242 cm^{-1} is assigned to the $\text{C}_{11}=\text{C}_{12}$ A_1 hydrogen rock combination that has moved down in frequency. The bands at 1182 and 1242 cm^{-1} are also observed (at 1182 and 1248 cm^{-1}) in the FTIR spectrum of the (meta-I)–(13-demethyl rhodopsin) difference.⁵³ The out-of-phase combination of the $\text{C}_{10}\text{--C}_{11}$ and $\text{C}_{12}\text{--C}_{13}$ stretches is expected to have very weak RR intensity because the $\text{C}_{10}\text{--C}_{11}$ stretch in 11-*cis* PSB starts out with weak intrinsic intensity which is further reduced by the out-of-phase contribution from the $\text{C}_{12}\text{--C}_{13}$ stretch. Therefore, the line at 1139 cm^{-1} probably represents an ionone ring vibration which has been observed in this region in all-*trans* retinal and β -ionone.⁴³ Finally, the lack of a mode at $\sim 1389\text{ cm}^{-1}$ in the RR spectrum of 13-demethyl rhodopsin (Figure 6C) is consistent with the absence of the 13-methyl group because this mode corresponds to the observed symmetric deformation of the 13-methyl group in unmodified 11-*cis* retinals (Figure 3A).⁴³

In the RR and FTIR spectra of 13-demethyl rhodopsin, there is no strong band between 960 and 990 cm^{-1} that could be assigned to a HOOP vibration. We conclude that the original $\text{C}_{11}=\text{C}_{12}$ A_2 HOOP mode has lost intensity in the 13-demethyl pigment. A perturbation of this mode is expected because the absence of the 13-methyl group allows the polyene to relax to a more planar conformation about the $\text{C}_{11}=\text{C}_{12}$ bond. This would in turn result in the reduction of the HOOP intensity,^{31,54} consistent with the RR spectrum (Figure 6) and the lower circular dichroism of its absorption band.^{21,45} In 11,12- D_2 rhodopsin (Figure 4), the downshift of the 970 cm^{-1} line reveals a peak at 976 cm^{-1} which has been attributed to the $\text{C}_7=\text{C}_8$ A_u HOOP vibration. Therefore, the residual line at 972 cm^{-1} in 13-demethyl rhodopsin is plausibly assigned to the $\text{C}_7=\text{C}_8$ A_u HOOP. The $\text{C}_{11}=\text{C}_{12}$ HOOP coordinate has most likely formed a combination with the $\text{C}_{13}=\text{C}_{14}$ HOOP coordinate and shifted up to 990 cm^{-1} (analogous to the coupling of the $\text{C}_7=\text{C}_8$, $\text{C}_9=\text{C}_{10}$, and $\text{C}_{11}=\text{C}_{12}$ HOOP vibrations in 9-demethyl rhodopsin).²¹ This HOOP combination is expected to show lower RR

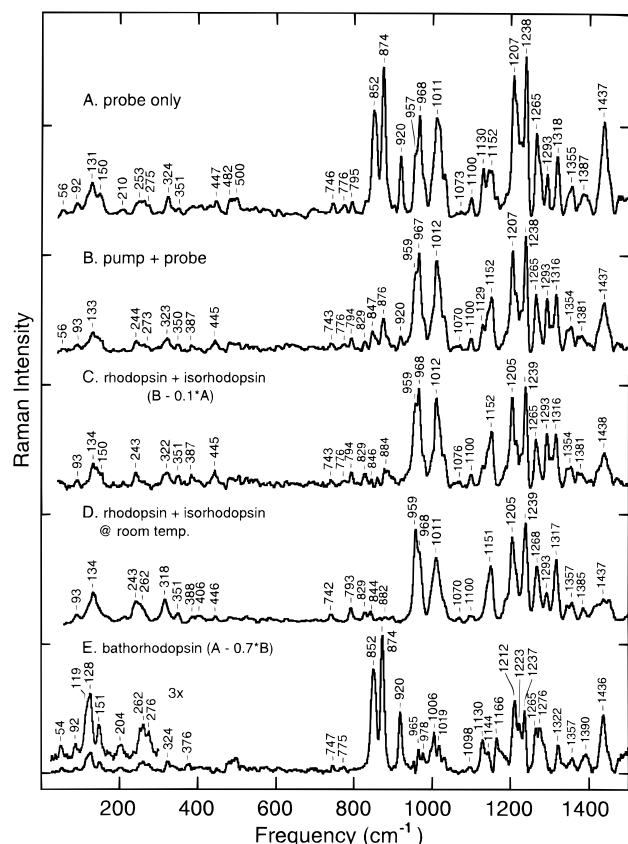


Figure 8. Resonance Raman spectra of rhodopsin frozen in glycerol–water glass at ~ 90 K. Spectrum obtained with (A) 488.0-nm (6.0 mW) probe excitation and (B) 488.0-nm (~ 1.0 mW) probe and 568.2-nm (~ 14 mW) pump excitations. (C) Spectrum of rhodopsin + isorhodopsin mixture at 90 K computed from the difference of pump + probe and probe-only spectra ($B - 0.1A$). (D) Sum of the room temperature spectra of rhodopsin (Figure 3A) and isorhodopsin (Figure 6A) in the proportion of 1 to 2. (E) Spectrum of bathorhodopsin at 90 K computed from the difference of probe-only and pump + probe spectra ($A - 0.7B$).

intensity because of the planar geometry of the 13-demethyl chromophore, as observed experimentally.

The 50–600 cm^{-1} Region. Four distinct peaks are detected at 128, ~ 247 , 328, and 440 cm^{-1} in 13-demethyl rhodopsin (Figure 7). The lines at 440 and 328 cm^{-1} are shifted by -6 and $+8$ cm^{-1} , respectively, from the nearest rhodopsin lines. The intensities of the 13-demethyl rhodopsin bands appear to be slightly lower compared to rhodopsin bands. The band at 247 cm^{-1} can be fit by a sum of three Lorentzian peaks at 215, 245, and 258 cm^{-1} . The 245- cm^{-1} band carries most of the intensity and appears very similar to the deconvoluted rhodopsin band at 246 cm^{-1} . A simple interpretation of the perturbation caused by the removal of the 13-methyl group is that the 260- cm^{-1} line in rhodopsin has lost intensity in the 13-demethyl analogue, leaving behind the peak at 245 cm^{-1} . There is also no Raman band in the 560- cm^{-1} region that corresponds to the rhodopsin line at 568 cm^{-1} . This line should be visible if its intensity is unchanged from that in rhodopsin because the signal-to-noise level is sufficient to detect a weak line nearby at 440 cm^{-1} .

Bathorhodopsin. Visible-light excitation of rhodopsin at temperatures below ~ 133 K creates a photostationary steady-state mixture of rhodopsin, isorhodopsin, and the primary photoproduct bathorhodopsin ($\lambda_{\text{max}} \sim 543$ nm). The RR spectrum (50–1500 cm^{-1}) obtained with 488.0-nm probe-only excitation (Figure 8A) is a superposition of the scattering from

each species in the proportion of 32% rhodopsin, 13% isorhodopsin, and 55% bathorhodopsin.^{38,55} The addition of a 568.2-nm pump beam (14:1 pump:probe power ratio) depletes the bathorhodopsin population by preferentially photoconverting it back to rhodopsin and isorhodopsin (Figure 1). This decrease is verified experimentally by the dramatic drop in the RR intensities at 852, 874, and 920 cm^{-1} which are due to the hydrogen wags of bathorhodopsin (Figure 8B).^{31,42} The composition under this condition is approximately 30% rhodopsin, 60% isorhodopsin, and 10% bathorhodopsin.^{38,56} Thus, between 950 and 1500 cm^{-1} , vibrational lines of rhodopsin and isorhodopsin, for example at 957, 968, 1207, 1238, 1265, and 1316 cm^{-1} , predominate in the pump + probe spectrum.

The RR spectra of the rhodopsin + isorhodopsin mixture and bathorhodopsin can be recovered by appropriate subtraction of the probe-only and pump + probe spectra. Subtracting a fraction ($\sim 10\%$) of the probe-only scan from the pump + probe scan until the 920- cm^{-1} bathorhodopsin line disappears produces a spectrum of the rhodopsin + isorhodopsin mixture at ~ 90 K (Figure 8C). This spectrum is nearly identical with a model spectrum generated by a superposition of the room temperature spectra of rhodopsin and isorhodopsin (Figures 3A and 6A) in the proportion of 1 to ~ 2 (Figure 8D). Similarly, the spectrum of bathorhodopsin is generated by subtracting a fraction of the pump + probe scan from the probe-only scan until the lines due to rhodopsin and isorhodopsin disappear (Figure 8E). This spectrum between 800 and 1500 cm^{-1} is identical to the spectrum of pure bathorhodopsin obtained using the spinning-cell technique.⁴²

The 50–600 cm^{-1} Region. The similarity of the low-frequency spectrum of the low-temperature rhodopsin + isorhodopsin mixture to its room temperature spectrum confirms that the subtraction procedure can accurately recover a spectrum of the low-frequency modes. The low-frequency region of bathorhodopsin contains distinct Raman-active peaks. Modes analogous to those in rhodopsin and isorhodopsin are located at 92, 128, 151, 262, and 324 cm^{-1} . Additional modes are detected at 119, 204, 276, and 376 cm^{-1} . There is also evidence of a weak band at 55–60 cm^{-1} . The assignment of this band to a bathorhodopsin mode is supported by the observation that the relative change in its intensity correlates almost directly with intensity changes of known bathorhodopsin lines at 852, 874, and 920 cm^{-1} (data not shown). Finally, lines near ~ 490 cm^{-1} may be residual glycerol bands (447 and 485 cm^{-1}) which are visible due to incomplete subtraction.

Protonated Schiff Bases. Figure 9 presents the complete solution Raman spectra of the 11-*cis* PSB, 13-demethyl, 11-*cis* PSB, and 9-*cis* PSB *n*-butylamine model compounds obtained with 750-nm excitation. The mode frequencies of the 11-*cis* and 9-*cis* PSB between 900 and 1700 cm^{-1} are identical, within the accuracy of the data, to their respective RR spectra acquired with 488-nm excitation.³³ The assignments of these vibrational modes are labeled in the figure. There are minor differences in the relative scattering intensities of some modes between the resonantly and nonresonantly excited spectra. The 970- cm^{-1} HOOP mode of the 11-*cis* PSB displays stronger relative scattering intensity under nonresonant excitation. In the 9-*cis* PSB spectra, the relative intensities of $\text{C}_{10}\text{--C}_{11}$, $\text{C}_{14}\text{--C}_{15}$, and $\text{C}_8\text{--C}_9$ stretches vary slightly.

In solution, the 11-*cis* PSB population can exist as two conformers by adopting either an *s-cis* or *trans* conformation about its $\text{C}_{12}\text{--C}_{13}$ bond to relieve steric interaction between 10H and 13-methyl groups. In polar solvents, the 12-*s-trans* species is the preferred conformer.⁵⁷ The vibrational bands observed

Rhodopsin and Isorhodopsin Preresonance Spectra. The Raman spectra of rhodopsin and isorhodopsin obtained with 792-nm excitation are shown in Figure 10. This wavelength corresponds to an energy that is $\sim 7300\text{ cm}^{-1}$ less than the λ_{max} of the $S_0 \rightarrow S_1$ electronic transition. The majority of the fundamental modes of rhodopsin and isorhodopsin, which are observed using resonant excitation, are also seen in the red-excitation data, but the relative intensities of some of them are altered. Figure 11 plots the ratio of the relative Raman scattering intensities of modes obtained with 792- and 488-nm excitations. In rhodopsin, relative Raman scattering by the 970-cm^{-1} HOOP mode and fingerprint modes at 1238 and 1268 cm^{-1} are about 10–20% greater under preresonance excitation. By contrast, modes at 246 , 320 , 446 , 997 , 1018 , 1606 , 1635 , and 1655 cm^{-1} display lower relative intensity off-resonance, whereas the scattering strengths of the 260 - and 568-cm^{-1} modes are approximately a factor of 2 greater. The HOOP and fingerprint modes of isorhodopsin also generally exhibit 10–20% greater scattering strength under 792-nm excitation, although the scattering by modes at 1141 and 1151 cm^{-1} appear significantly greater. Relative scattering by modes at 242 , 315 , $351 \sim 1010$, 1599 , 1635 , and 1654 cm^{-1} are weaker in the preresonance spectrum of isorhodopsin.

TABLE 1: Normal Modes of the 11-*cis* Retinal PSB Chromophore of Rhodopsin. Comparison with QCFF/PI Calculated Mode Frequencies, Relative Raman Intensities, and Excited-State Displacements

mode (cm ⁻¹)		assignment	<i>I</i> / <i>I</i> ₁₅₄₈ ^d	Δ ^e
obs	calc ^a			
93		skeletal torsion	0.022	0.90
131		skeletal torsion	0.15	1.61
246		CCC A ₁ bend	0.11	0.95
260		C ₁₀ –C ₁₃ A ₂ skeletal torsion	0.105	0.94
321		skeletal torsion	0.048	0.73
410			0.026	0.31
446			0.028	0.30
568	543	C ₁₁ =C ₁₂ A ₂ torsion	0.023	0.30
745		ionone ring vibration	0.021	<i>g</i>
– (762 ^b)	736	C ₁₁ =C ₁₂ B ₂ HOOP ^b		
793		ionone ring vibration	0.023	0.20
843 (838 ^b)	848	C ₇ =C ₈ B _g HOOP + 10H wag ^b	0.040	0.29
866 (869 ^b)	941	14H wag + NH wag ^b	<0.01	<i>g</i>
882 (882 ^b)	899	10H wag – C ₇ =C ₈ B _g HOOP ^b	<0.01	<i>g</i>
970	976	C ₁₁ =C ₁₂ A ₂ HOOP – C ₁₁ =C ₁₂ torsion ^c	0.26	0.57
976 (965 ^b)	968	C ₇ =C ₈ A _u HOOP + C ₇ =C ₈ torsion ^c	<i>f</i>	<i>g</i>
– (992 ^b)	1000	15H wag ^b		
997 (996 ^b)	1006	13-methyl rock ^{b,c}	0.043	0.17
1012			0.05	<i>g</i>
1018 (1017 ^b)	1037	9-methyl rock ^b	0.08	0.45
1098	1104	C ₁₀ –C ₁₁ stretch ^c	0.026	0.17
1190	1181	C ₁₄ –C ₁₅ stretch ^c	0.029	0.30
1214	1224	C ₈ –C ₉ stretch ^c	0.21	0.45
1238	1234	C ₁₂ –C ₁₃ stretch + 14H rock ^c	0.25	0.46
1268	1268	11H–12H A ₁ rock ^c	0.23	0.48
1318			0.027	0.20
1357			0.023	0.24
1389	1389	13-methyl symmetric deform ^b	0.024	0.17
1428			0.040	<i>g</i>
1435			0.043	0.22
1451			0.042	0.17
1548 (1543 + 1551)	1579	in-phase C=C stretch ^c	1.000	0.88
1578			0.087	0.20
1606		C=C stretches ^{b,c}	0.084	0.31
1635			0.021	0.23
1655	1653	C=N stretch ^c	0.069	0.26

^a Mode frequency obtained from vibrational analysis using the QCFF/PI program. ^b Assignment from 11-*cis* retinal.⁴³ ^c Assignment from Eyring et al.³¹ and Palings et al.³³ ^d Resonance Raman scattering intensity of a mode relative to the intensity of the in-phase ethylenic stretch mode at 1548 cm⁻¹. Average error of the ratio is ~15%. ^e Excited-state displacements (Δ 's) from resonance Raman intensity analysis by Wexler and Mathies.⁷⁶ Homogeneous Gaussian and inhomogeneous widths were 330 cm⁻¹ (fwhm) and 615 cm⁻¹ (fwhm), respectively. The electronic 0–0 energy was 18 130 cm⁻¹, the transition moment length was 2.114 Å, and the temperature was 277 K. ^f No detectable scattering intensity. ^g Not included in the Raman intensity calculation.

Normal Mode Analyses of 11-*cis* Retinal PSB and Analogues. The normal modes of the 11-*cis* retinal PSB were calculated using the QCFF/PI method in order to characterize its low-frequency vibrations. The normal modes were computed for the energy-minimized 11-*cis* PSB structure (Figure 2). Its ground-state C₆–C₇ dihedral angle is twisted by ~36° to minimize nonbonded interaction between the 5-methyl group and the C₈ hydrogen, consistent with the ~41° angle determined from X-ray^{59,60} and NMR⁶¹ structures of 11-*cis* retinal. The steric hindrance between the 10H and 13-methyl groups in the 12-*s-trans* conformer is likewise accommodated by a ground-state torsion of ~22° about the C₁₂–C₁₃ bond.

The QCFF/PI-calculated in-plane and out-of-plane modes above 750 cm⁻¹ are compared with known assignments of the characteristic vibrational bands of 11-*cis* retinal⁴³ and its PSB^{31,33} in Table 1. Vibrational assignments of calculated normal modes were made on the basis of the magnitude of the coefficients of internal coordinates which make up a normal mode. The frequencies of the major in-plane vibrations such as the 11H–12H A₁ rock and the C=C and C–C stretches are in good agreement with the experimental numbers. The C₁₁=C₁₂ A₂ HOOP is placed correctly at ~970 cm⁻¹, but its B₂ frequency is predicted about 30 cm⁻¹ lower. The QCFF/PI frequencies

of the A_u and B_g species of the C₇=C₈ coupled HOOP and 10H wag are also consistent with the empirical assignments. The frequency of the 14H + NH wag combination is not accurate, and this discrepancy may be due to the fact that the π -electron system of heteroatoms is not modeled accurately. On the whole, the calculated normal modes are in good agreement with the empirical assignments, demonstrating that the QCFF/PI method does a good job of qualitatively modeling the kinetic and potential couplings of the in-plane and out-of-plane vibrations in retinal polyenes.

Internal coordinate descriptions for a representative set of low-frequency normal modes (<800 cm⁻¹) calculated for the 11-*cis* PSB are listed in Table 2. CCC bending coordinates make a strong contribution to vibrations between ~750 and 500 cm⁻¹. For example, the C₁₁C₁₂C₁₃ bend is the dominant internal coordinate of the 754-cm⁻¹ mode which is best described as a localized bending vibration. Other bending modes at lower frequencies (666, 648, 609, 572, 511 cm⁻¹) are linear combinations of several CCC coordinates with similar coefficients and, thus, represent delocalized in-plane deformations. Ethylenic torsions constitute the primary internal coordinates of modes at 543 cm⁻¹ and between 500 and 400 cm⁻¹. The 543-cm⁻¹ mode is unique in that it is calculated to consist of a single

TABLE 2: Selected Low-Frequency Normal Modes from the Vibrational Analysis of the 11-*cis* Retinal PSB

mode (cm ⁻¹)	internal coordinate description ^a		
	bend	torsion	wag
754	0.190 β (11,12,13) - 0.115 β (10,11,12) - 0.113 β (12,13,Me)		
666	-0.102 β (6,7,8) - 0.091 β (Me,9,10) + 0.076 β (9,10,11)	0.293 τ (6-7) - 0.146 τ (7=8)	
648	0.103 β (9,10,11) - 0.090 β (7,8,9) - 0.0813 β (13,14,15)	-0.260 τ (6-7) + 0.139 τ (8-9)	
609	0.127 β (13,14,15) - 0.087 β (9,10,11) + 0.079 β (12,13,14)		
572	0.132 β (8,9,Me) + 0.101 β (12,13,14)	0.077 τ (11=12) - 0.053 τ (12-13)	
543	0.043 β (12,13,Me) + 0.035 β (11,12,13) + 0.033 β (8,9,Me)	-0.538 τ (11=12) + 0.235 τ (14-15) + 0.137 τ (13=14)	0.543w(13Me) - 0.113w(9Me) - 0.225w(11H) + 0.176w(12H)
511	-0.111 β (Me,9,10) + 0.093 β (8,9,10) - 0.062 β (10,11,12)	-0.113 τ (7=9) + 0.097 τ (10-11) + 0.052 τ (15=N)	0.229w(9Me) + 0.068w(11H) - 0.062w(7H)
483	0.098 β (14,15,N) + 0.060 β (8,9,Me)	-0.202 τ (10-11) + 0.148 τ (11=12) + 0.108 τ (7=8) + 0.093 τ (8-9) - 0.092 τ (9=10)	-0.355w(9Me) - 0.165w(13Me) + 0.112w(11H) + 0.108w(7H)
456	-0.089 β (12,13,Me) + 0.087 β (Me,13,14) + 0.066 β (10,11,12) - 0.064 β (8,9,10)	0.204 τ (11=12) - 0.172 τ (12-13) + 0.106 τ (15=N) + 0.100 τ (14-15) - 0.084 τ (10-11) - 0.081 τ (13=14)	0.087w(12H) + 0.112w(11H) + 0.081w(13Me)
442	0.081 β (8,9,Me) - 0.076 β (Me,13,14) - 0.060 β (10,11,12)	-0.189 τ (11=12) + 0.177 τ (12-13) - 0.118 τ (14-15) - 0.099 τ (15=N) + 0.092 τ (13=14) + 0.091 τ (10-11)	-0.118w(13Me) - 0.077w(14H) - 0.089w(11H) + 0.079w(12H)
404	0.073 β (Me,12,13)	0.325 τ (11=12) - 0.299 τ (12-13) + 0.156 τ (14-15) - 0.150 τ (9=10) - 0.143 τ (10-11) - 0.113 τ (13=14)	0.205w(13Me) - 0.173w(12H) + 0.107w(14H) + 0.091w(11H)
353	0.068 β (8,9,Me) - 0.057 β (12,13,Me)	0.112 τ (10-11) + 0.097 τ (7=8) - 0.080 τ (11=12) + 0.076 τ (12-13) - 0.067 τ (6-7) - 0.064(15=N)	0.075w(9Me) - 0.070w(8H) - 0.053w(11H)
282	0.053 β (Me,9,10) + 0.034 β (14,15,N) + 0.032 β (11,12,13)	-0.139 τ (15=N) + 0.125 τ (8-9) - 0.124 τ (10-11) + 0.103 τ (13=14) - 0.092{ τ (6-7) + τ (12-13)} + 0.073 τ (11=12)	0.063w(13Me) - 0.066w(10H) + 0.051w(11H)
228		-0.115 τ (8-9) + 0.105 τ (6-7) + 0.093 τ (10-11) + 0.087 τ (15=N) - 0.080 τ (11=12) - 0.077 τ (13=14) + 0.068 τ (12-13)	
220		0.139 τ (6-7) - 0.122 τ (8-9) + 0.063 τ (10-11) - 0.051 τ (11=12) + 0.050 τ (15=N)	
204		-0.095 τ (9=10) - 0.076 τ (14-15) + 0.052 τ (10-11) + 0.050 τ (12-13)	0.053w(19H) - 0.040w(9Me)
187		-0.106 τ (14-15) - 0.79 τ (8-9) - 0.061 τ (15=N)	0.055w(13Me)
182		0.219 τ (14-15) - 0.58 τ (8-9)	
152		0.144 τ (8-9) - 0.107 τ (6-7) + 0.066 τ (12-13) - 0.053 τ (14-15) + 0.052 τ (15=N)	
145	0.040 β (8,9,Me)	0.037 τ (8-9) - 0.037 τ (10-11) + 0.014 τ (13=14) - 0.013 τ (15=N) - 0.011 τ (14-15) - 0.011 τ (6-7)	
132		0.065 τ (15=N) - 0.055 τ (9=10) + 0.045 τ (12-13) - 0.036 τ (14-15) + 0.025 τ (13=14) - 0.017 τ (6-7) - 0.011 τ (11=12)	
111		-0.075 τ (10-11) + 0.056 τ (6-7) + 0.054 τ (9=10) - 0.037 τ (14-15) - 0.036 τ (12-13) - 0.036 τ (8-9) - 0.024 τ (7=8) + 0.022 τ (11=12) + 0.014 τ (13=14)	-0.033w(10H)
87, 78, 52 } 45, 41 }		delocalized out-of-plane skeletal twisting	

^a Tabulated values are coefficients of internal coordinate projections along the normal mode coordinate. Abbreviations: $\beta(x, y, z) = C_x C_y C_z$ bend, $\tau(x-y) = C_{x-1} C_x C_y C_{y+1}$ single bond torsion, $\tau(x=y) = C_{x-1} C_x C_y C_{y+1}$ double bond torsion, w = wag, Me = methyl carbon.

dominant torsion of the $C_{11}=C_{12}$ bond that is also mixed strongly with its A_2 HOOP vibration. Vibrations at 483, 456, 442, and 404 cm^{-1} possess smaller projections along the $\tau(C_{11}=C_{12})$ coordinate and represent more delocalized motions involving torsions primarily of $C_9=C_{10}$, $C_{13}=C_{14}$, $C_{10}-C_{11}$, $C_{12}-C_{13}$, and/or $C_{14}-C_{15}$ bonds. The internal coordinate compositions of modes between ~ 350 and $\sim 220 \text{ cm}^{-1}$ show that they are mixtures of several $\tau(C=C)$ and $\tau(C-C)$ coordinates. A subset of these at 353, 282, 242, and 228 cm^{-1} also contain a small degree of $\tau(C_{11}=C_{12})$ character. Generally, the relative magnitudes of $\tau(C-C)$ character in the torsional modes increase with decreasing frequency. For instance, the relative contributions from $C_{10}-C_{11}$ and $C_{12}-C_{13}$ torsions are comparable to those of $\tau(C=C)$ coordinates in the modes at 353, 282, 242, and 228 cm^{-1} . Vibrations between ~ 250 and $\sim 150 \text{ cm}^{-1}$ mostly consist of C-C torsions. Modes below 150 cm^{-1} consist of many $\tau(C-C)$ and $\tau(C=C)$ coordinates with similar coefficients, resulting in a delocalized small-amplitude skeletal twisting of the polyene. These calculated vibrational modes of the 11-*cis* PSB are similar to those of 11-*cis*, 12-*s-cis* retinal,²⁰ and also consistent with vibrations expected from analyses on *cis*-stilbene^{62,63} and simple polyenes such as butene, butadiene, and hexatriene. The frequencies of in-plane CCC bending^{43,64-66} and double bond torsional^{43,64,66} vibrations range between 200 and 600 cm^{-1} , and single bond torsional and skeletal twisting modes are usually found below $\sim 200 \text{ cm}^{-1}$.^{43,66,67}

The calculated effects of isotopic substitutions on the low-frequency modes of the 11-*cis* PSB which carry $\tau(C_{11}=C_{12})$ character are summarized in Figure 5B. Overall, deuterium substitutions at C_{11} and C_{12} induce the largest frequency shifts, as expected. This is most apparent in the $C_{11}=C_{12}$ A_2 HOOP vibration which is calculated to move down by 203 cm^{-1} , close to the shift of 186 cm^{-1} seen in rhodopsin.³¹ The 543- cm^{-1} torsional mode is predicted to downshift $\sim 23 \text{ cm}^{-1}$ because it is strongly mixed with the A_2 HOOP. Furthermore, because this mode involves torsional and CCC bending motion between C_{12} and C_{14} , ^{13}C substitutions at $C_{12}-C_{13}$ and $C_{13}=C_{14}$ bonds also cause downshifts of $\sim 8 \text{ cm}^{-1}$. The mode at 404 cm^{-1} which has the second largest $\tau(C_{11}=C_{12})$ coefficient shifts down $\sim 15 \text{ cm}^{-1}$ in 11,12- D_2 retinal and by $\sim 3 \text{ cm}^{-1}$ in the di- ^{13}C retinals. Other modes are comparatively less sensitive to the isotopic substitutions, consistent with the smaller coefficients of $\tau(C_{11}=C_{12})$ and $C_{11}=C_{12}$ A_2 HOOP coordinates in their normal mode vector. Three $\tau(C=C)$ modes near 450 cm^{-1} are shifted on average by ~ 6 and $\sim 1.5 \text{ cm}^{-1}$ by 11,12- D_2 and ^{13}C substitutions, respectively. These shifts nevertheless are still a few wavenumbers greater than those calculated for vibrations which have a very small projection along internal coordinates between C_{10} and C_{14} . For example, the modes at 499 and 508 cm^{-1} are calculated to shift by less than 6 and 0.5 cm^{-1} by 11,12- D_2 and ^{13}C substitutions, respectively (data not shown). Below 400 cm^{-1} , most of the modes undergo shifts of ~ 3 and $\sim 1 \text{ cm}^{-1}$ or less in 11,12- D_2 and di- ^{13}C retinals, respectively, because these vibrations are delocalized and many coordinates make approximately equal contribution. Results from the calculations indicate that a large isotopic shift, especially that induced in modes above 400 cm^{-1} by deuterium substitutions at C_{11} and C_{12} , are correlated with modes that have large components of $C_{11}=C_{12}$ torsional character. Below 400 cm^{-1} , a shift is indicative of atomic motion of the C_{10} -to- C_{14} region, but the delocalized nature of these vibrations preclude assignments to specific coordinate(s) with confidence.

Normal mode calculations have also been carried out on the 9-demethyl and 13-demethyl analogues of 11-*cis* PSB to

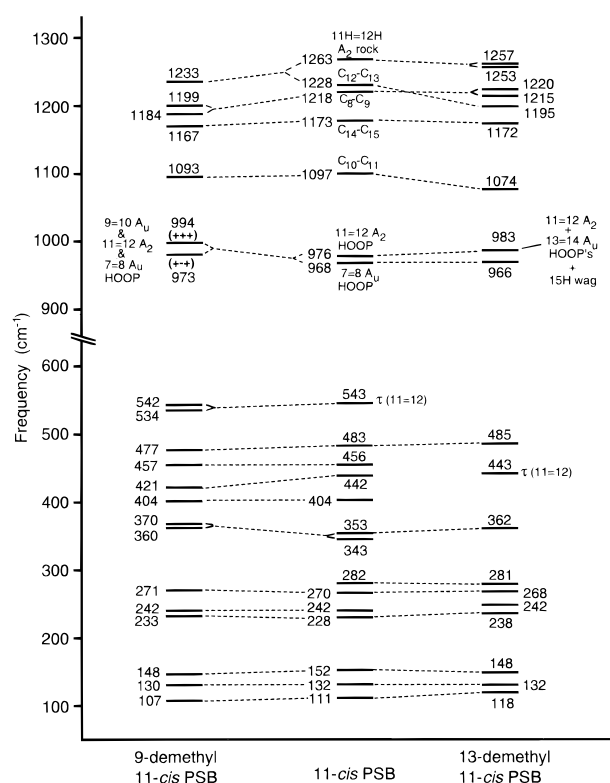


Figure 12. Correlation diagram of the fingerprint and low-frequency modes calculated for the 11-*cis* PSB, 9-demethyl 11-*cis* PSB, and 13-demethyl 11-*cis* PSB using the QCFF/PI method.

examine the effects of the removal of a methyl group on their structures and vibrations. The energy-minimized geometry of the 9-demethyl, 11-*cis* PSB is unchanged from that of unmodified 11-*cis* PSB because the 9-methyl group does not participate in intramolecular nonbonded interactions (Figure 2). In contrast, the removal of the 13-methyl group results in a planarization of the polyene geometry.

The vibrations of the 11-*cis* PSB and its demethyl analogues are compared in Figure 12. The calculation qualitatively reproduces the change in kinetic coupling caused by the loss of the C-CH₃ stretching coordinate and the resulting drop in the frequency of the adjacent C-C stretching mode. However, the magnitude of this decrease is slightly smaller than that observed experimentally. An $\sim 20\text{-cm}^{-1}$ downshift of the C_8-C_9 stretching mode is predicted in the 9-demethyl PSB, and the mode with $C_{12}-C_{13}$ stretch character in the 13-demethyl PSB is expected to be $\sim 30 \text{ cm}^{-1}$ lower than that in the 11-*cis* PSB (Figure 6). Furthermore, the loss of the methyl group allows previously isolated hydrogen wag coordinates to mix. In the 9-demethyl PSB, the $C_7=C_8$ A_u and $C_{11}=C_{12}$ A_2 HOOPs couple with the new $C_9=C_{10}$ HOOP to form an in-phase (+ + +) combination at 994 cm^{-1} and a (+ - +) combination at 973 cm^{-1} . In the 13-demethyl PSB, a HOOP mode consisting of the $C_{11}=C_{12}$ A_2 HOOP, $C_{13}=C_{14}$ A_u HOOP, and 15H wag coordinates is calculated at 983 cm^{-1} , but the $C_7=C_8$ A_u HOOP frequency is unchanged at $\sim 966 \text{ cm}^{-1}$ because the 9-methyl group still isolates this vibration from other wags.

Low-frequency vibrations of the 11-*cis* PSB with $\tau(C_{11}=C_{12})$ character have been correlated to those of the 9-demethyl PSB and 13-demethyl PSB. The 11-*cis* PSB vibrations correlate well with those in the 9-demethyl, 11-*cis* PSB, indicating that the absence of the 9-methyl group does not qualitatively alter the pattern in the low-frequency region. On the other hand, the removal of the 13-methyl group perturbs the C=C torsional

modes previously identified with strong $\tau(\text{C}_{11}=\text{C}_{12})$ character. There is no longer a localized $\tau(\text{C}_{11}=\text{C}_{12})$ mode near 540 cm^{-1} , and only two modes with large $\tau(\text{C}_{11}=\text{C}_{12})$ character are predicted at 485 and 443 cm^{-1} . The 485-cm^{-1} mode correlates with the one at the same frequency in 11-*cis* PSB. The mode at 443 cm^{-1} has the largest $\tau(\text{C}_{11}=\text{C}_{12})$ torsion coefficient in the 13-demethyl PSB. However, this vibration is also mixed with torsions of the $\text{C}_9=\text{C}_{10}$, $\text{C}_{10}-\text{C}_{11}$, $\text{C}_{12}-\text{C}_{13}$, and $\text{C}_{13}=\text{C}_{14}$ bonds and, hence, is not strictly correlated with any of the 11-*cis* PSB modes. The vibrational analyses on the 9-demethyl and 13-demethyl PSB's indicate that removal of the 13-methyl group preferentially perturbs the $\text{C}_{11}=\text{C}_{12}$ torsional vibrations. Similarly, vibrational properties of modes which involve $\text{C}_9=\text{C}_{10}$ torsions are affected more by the removal of the 9-methyl group (data not shown).

Discussion

The spectral region below 600 cm^{-1} in the RR spectrum of rhodopsin is characterized by a series of well-resolved bands due to normal modes with significant RR scattering strengths. The most intense is the broad band centered at 255 cm^{-1} which is a composite of two overlapping lines due to modes at 246 and 260 cm^{-1} . There is a mode of lower intensity at 131 cm^{-1} , and weaker bands are also detected at 93 , 320 , 446 , and 568 cm^{-1} . In conjugated polyenes, the principal types of nuclear motions at these low frequencies are single and double bond torsions and CCC bends.²⁰ Since the RR intensity of a mode reflects the extent of initial dynamics along that coordinate on the excited-state surface, the scattering activities of these modes indicate that the photoexcited 11-*cis* chromophore immediately undergoes significant skeletal twisting. Loppnow and Mathies¹⁰ suggested that one or more of these modes may be reporting on the torsional dynamics of the 11-*cis* PSB chromophore along the reactive $\text{C}_{11}=\text{C}_{12}$ isomerization coordinate. The identification of modes which contain $\text{C}_{11}=\text{C}_{12}$ torsional character and the quantitation of their RR cross-sections will allow one to probe the shape of the excited-state surface in the Franck-Condon region and to reconstruct the initial nuclear motions involved in the isomerization. Such an analysis is now critically important for understanding the mechanism of the 200-fs isomerization in vision because we now have evidence that *initial* nuclear dynamics may be directly related to the motion to the transition state and beyond. However, a more detailed and quantitative analysis was not possible in the earlier study because the vibrational mode assignments had not been determined.

We have undertaken the present study to assign the low-frequency normal modes of rhodopsin in order to deduce the initial excited torsional dynamics of the chromophore and to understand the mechanism of this fast and efficient photochemistry. 11-*Cis* retinals were synthesized with specific isotopic substitutions and used to obtain Raman spectra of regenerated pigments as well as of the protonated Schiff base model compounds. The correlation of the experimental isotopic frequency shifts with the shifts predicted by a vibrational analysis of the 11-*cis* PSB suggests specific normal mode assignments for the observed Raman-active low-frequency bands. These assignments are also shown to be consistent with assignments inferred from the analysis of the symmetry species of the Raman bands. We first discuss the normal mode assignments in rhodopsin. Then these assignments and spectral intensities are used to provide a better understanding of the initial photochemical torsional dynamics in rhodopsin.

Rhodopsin Normal Modes. One of the unique properties of retinals and their PSB's from the viewpoint of vibrational

analysis is the localized nature of their molecular vibrations. This has made it possible to identify specific normal modes whose frequencies and/or intensities are sensitive to the local geometry or geometry changes and are thus diagnostic of the chromophore's isomeric state and excited-state dynamics.^{32,43} These signature Raman bands can be recognized from the comparison of the Raman spectra of the 9-*cis* and 11-*cis* PSB's (Figure 9). The 11-*cis* configuration gives rise to intense distinctive bands at ~ 970 and 1273 cm^{-1} that are due to the HOOP and rocking vibrations, respectively, of the 11H and 12H atoms. In addition, the $\text{C}_{10}-\text{C}_{11}$ stretching mode is located at 1098 cm^{-1} with negligible intensity. In the 9-*cis* PSB, the $\text{C}_{10}-\text{C}_{11}$ stretch shows much stronger intensity and is shifted up by $\sim 45\text{ cm}^{-1}$. The 9-*cis* spectrum also displays a prominent 8H rocking mode at 1329 cm^{-1} and a weaker $\text{C}_7=\text{C}_8$ HOOP mode at $\sim 960\text{ cm}^{-1}$. These differences are also evident in the resonance (Figures 3A and 6A) and preresonance (Figure 10) spectra of the 9-*cis* and 11-*cis* chromophores in isorhodopsin and rhodopsin.

A similar comparison applied to the low-frequency regions of rhodopsin and isorhodopsin shows that the modes at 246 , 260 , 446 , and 568 cm^{-1} are unique to rhodopsin and the 11-*cis* chromophore. The $\text{C}_{11}=\text{C}_{12}$ HOOP mode at 970 cm^{-1} is unique to rhodopsin, and its strong RR intensity is suggestive of torsional motion of the $\text{C}_{11}=\text{C}_{12}$ bond.³¹ The 9-*cis* chromophore in isorhodopsin isomerizes about the $\text{C}_9=\text{C}_{10}$ bond, but the HOOP vibration showing strong intensity is that of 7H and 8H. Therefore, the observation that the four low-frequency modes at 246 , 260 , 446 , and 568 cm^{-1} , like the $\text{C}_{11}=\text{C}_{12}$ HOOP mode, are detected in rhodopsin suggests that one or more of them may represent motion along the reactive $\text{C}_{11}=\text{C}_{12}$ torsion and/or report on the dynamics along other torsional coordinates associated with the isomerization. Conversely, modes that are common to both rhodopsin and isorhodopsin most likely reflect vibrations of the part of the polyene that have similar geometry or structure in the two isomers. The modes at 93 , 131 , 320 , and 585 cm^{-1} belong to this group.

Vibrational Character of the Low-Frequency Modes. Of the four low-frequency modes of interest, the 568-cm^{-1} mode is most perturbed by the isotopic substitutions. Its frequency drops by $\sim 35\text{ cm}^{-1}$ in 11,12- D_2 rhodopsin and by $\sim 8\text{ cm}^{-1}$ in the 12,13- d_2^{13}C and 13,14- d_2^{13}C derivatives. In fact, its vibrational correlation pattern uniquely resembles the pattern predicted for the localized $\text{C}_{11}=\text{C}_{12}$ torsional mode that is calculated at 543 cm^{-1} . The experimental and calculated ^{13}C -induced shifts are in good agreement. However, the 11,12- D_2 shift calculated for the 543-cm^{-1} mode is smaller than the experimental shift by 12 cm^{-1} , suggesting that the vibrational calculation underestimates the amount of $\text{C}_{11}=\text{C}_{12}$ torsional and/or HOOP vibrational character in this mode. Nevertheless, none of the other calculated modes of the 11-*cis* PSB exhibits isotopic shifts of similar magnitude. On the basis of the isotope data, we assign the 568-cm^{-1} mode in rhodopsin to the relatively localized $\text{C}_{11}=\text{C}_{12}$ torsional vibration.

The $\text{C}_{11}=\text{C}_{12}$ torsional assignment for the 568-cm^{-1} mode is also consistent with the behavior of the localized $\text{C}_{11}=\text{C}_{12}$ torsion mode in the demethyl analogue chromophores. One would expect a priori on the basis of simple reduced-mass effects that the removal of the 13-methyl group would perturb the $\text{C}_{11}=\text{C}_{12}$ torsional vibration more than removal of the 9-methyl group. This idea is supported by QCFF/PI calculations on the 9-demethyl and 13-demethyl 11-*cis* PSB analogues. As illustrated in Figure 12, the removal of the 9-methyl has no major effect on the pattern of the low-frequency modes that contain

$C_{11}=C_{12}$ torsional character. In particular, a localized $C_{11}=C_{12}$ torsion mode is calculated at the same frequency as that in the 11-*cis* PSB. There is also another torsional mode with slightly smaller $C_{11}=C_{12}$ character that appears at 534 cm^{-1} . The removal of the 13-methyl group, on the other hand, results in the loss of several torsional modes. Most importantly, there is no longer a localized $C_{11}=C_{12}$ torsional mode near 540 cm^{-1} in the 13-demethyl PSB. The mode with the largest $C_{11}=C_{12}$ torsional component is calculated at 443 cm^{-1} instead, and it is not correlated to the localized $C_{11}=C_{12}$ mode of the 11-*cis* PSB. Consistent with the results of the calculations, only 9-demethyl rhodopsin displays a strong mode at 570 cm^{-1} that corresponds to the 568-cm^{-1} $C_{11}=C_{12}$ torsional mode of native rhodopsin (Figure 7).

Evaluating the vibrational character of the remaining low-frequency modes is not as straightforward because none of their isotopic-shift correlation diagrams exhibits a distinctive pattern. The reason for the nondistinctive shift pattern is that these modes are delocalized vibrations. This is obvious when one examines the composition of the QCFF/PI normal modes below $\sim 450\text{ cm}^{-1}$ (Table 2). Many coordinates with similar amplitudes contribute to the total vibration. As a result, an isotopic labeling at only one of the coordinates does not perturb the overall vibration enough to cause frequency shifts of the magnitude observed for the more localized $C_{11}=C_{12}$ HOOP and torsional modes. Nevertheless, an inspection of the mode description suggests that a shift induced by the 11,12- D_2 label is large enough to interpret and is associated with contributions from vibrational coordinates between C_{10} and C_{13} . The rhodopsin mode at 260 cm^{-1} downshifts 7 cm^{-1} in the 11,12- D_2 derivative spectrum and 2 cm^{-1} in the spectrum of the chromophore labeled with ^{13}C at the $C_{10}-C_{11}$ or $C_{12}-C_{13}$ bond. No mode in the calculation qualitatively reproduces this experimental shift pattern. However, on the basis of our knowledge of molecular vibrations in retinals, the shifts of the 260-cm^{-1} mode in 11,12- D_2 , 10,11- $d^{13}\text{C}$, and 12,13- $d^{13}\text{C}$ derivatives are consistent with those of a mode that involves some combination of $C_{10}-C_{11}$, $C_{11}=C_{12}$, and $C_{12}-C_{13}$ torsions and 11H and 12 H wags. Its $C_{11}=C_{12}$ torsional character is obviously much weaker compared to that in the 568-cm^{-1} mode. The mode at 246 cm^{-1} also involves motion of the $C_{12}-C_{13}$ coordinate since its frequency is sensitive to the 12,13- $d^{13}\text{C}$ and 11,12- D_2 substitutions.

Symmetry Species of the Low-Frequency Modes. The in-plane and out-of-plane normal modes are distinguishable by their symmetry labels. In a planar unsubstituted polyene, the symmetry species of out-of-plane modes such as torsions and wags may be A_u or B_g in the C_{2h} point group and A_2 or B_1 in the C_{2v} point group. The Raman selection rules, in turn, specify which symmetry species can undergo a Raman transition. Given these rules, one way to differentiate between in-plane and out-of-plane vibrations is by correlating the experimental pattern of Raman intensities of an unassigned band to the pattern predicted for a vibration of a particular symmetry.

Strictly speaking retinals and their protonated Schiff bases lack symmetry and belong to the C_1 point group. However, because their electronic and vibrational properties are primarily dictated by properties of the conjugated system, they are ascribed approximate point group labels based on the transformation properties of the polyene.^{16,68} These approximate symmetry labels are useful for qualitative prediction and understanding of the behaviors of the electronic states and vibrational modes of retinals. The point group of all-*trans* retinal and its PSB can be approximated as " C_{2h} ". The point group of an idealized planar 11-*cis* retinal and its PSB may be

approximated as " C_{2v} ".⁶⁹ However, the actual geometry of 11-*cis* retinal is distorted because of the steric interaction between the 10H and the 13-methyl group. If this deformation is assumed to occur mostly along the $C_{11}=C_{12}$ bond, then the symmetry about the C_2 -axis is roughly preserved and the molecular point group may be ascribed the next lower symmetry of C_2 . In the following discussion, to illustrate the effects of increasing molecular asymmetry on the Raman activities of the in-plane and out-of-plane normal modes, it will be adequate to approximate the point group of 11-*cis* retinal and its PSB as C_2 .

We first discuss what is expected for a simple polyene in the higher symmetry C_{2v} group. A torsional internal coordinate has A_2 symmetry in this group.⁷⁰ The symmetry species of a torsional normal mode which is a linear combination of torsional internal coordinates and other out-of-plane coordinates may be either A_2 or B_1 . Modes of neither symmetry will show *resonance* Raman intensity because only totally symmetric (A_1) normal modes may scatter via the resonant "A-term" process.^{24-26,71} A_2 or B_1 modes will exhibit Raman intensity away from resonance when scattering mechanisms that involve vibronic coupling of allowed and forbidden electronic states begin to dominate over the A-term process.⁷² However, in a planar polyene, the magnitude of this off-resonance scattering by out-of-plane modes (A_2 or B_1) will still be weak relative to the scattering by in-plane modes (A_1 or B_2) because the in-plane component of the electronic transition moment is much larger than its out-of-plane component.

When the molecular symmetry drops from C_{2v} to C_2 due to a loss of reflection symmetry because of a distortion in the ground-state geometry, the available symmetry species collapse to just A or B. The torsional modes which were originally A_2 now belong to the totally symmetric species (A) and are RR active. In physical terms, the distortion introduces or augments the molecular polarizability in the direction orthogonal to the polyene plane by mixing out-of-plane electronic character into the allowed planar electronic states. A large change in Raman scattering strength will be restricted to a subset of out-of-plane normal modes which project along internal coordinates whose ground-state equilibrium positions are displaced by the ground-state distortion. The intensities of both the on- and off-resonance scattering by out-of-plane modes will reflect the degree of the out-of-plane distortion.

The change in the Raman selection rules that accompanies symmetry lowering can also be utilized to identify normal modes of rhodopsin that correspond to torsional vibrations. In this analysis, we will make use of the idea that the 13-demethyl rhodopsin, which has a planar polyene geometry, can be regarded as a model 11-*cis* analogue that belongs to the C_{2v} point group. The resonance Raman activity of the 970-cm^{-1} HOOP mode in rhodopsin will be discussed first to illustrate how the RR intensity of an A_2 mode varies with molecular structure.

In the C_{2v} point group, the A_2 -coupled HOOP internal coordinate of a *cis* double bond is composed of the out-of-plane wagging motions of the two hydrogens in opposite directions. This mode has the same symmetry as that of a torsion coordinate. The molecular vibrations of retinals, including HOOP vibrations (i.e. $\text{HC}_7=\text{C}_8\text{H}$, 10H, $\text{HC}_{11}=\text{C}_{12}\text{H}$, 14H, 15H, NH) are relatively localized compared to those in unsubstituted polyenes because kinetic coupling between internal coordinates that are separated by the methyls at C_9 and C_{13} are weaker.^{43,55} As a result, the vibrational character of certain normal modes may be described by the vibrations of a few (1–3) dominant

internal coordinate(s). The $C_{11}=C_{12}$ coupled HOOP normal mode in the 11-*cis* PSB is made up of mostly this A_2 HOOP coordinate and a smaller amount of the $C_{11}=C_{12}$ torsion. Its symmetry species, therefore, can be assigned as A_2 . An analogous HOOP mode in the 13-demethyl PSB contains slightly more 15H was character due to the absence of the 13-methyl group, but the A_2 $C_{11}=C_{12}$ HOOP coordinate is still the dominant component. In a " C_{2v} " molecule like the 13-demethyl PSB, a RR transition (via a Condon mechanism) in this HOOP normal coordinate is forbidden by symmetry. Consistent with this expectation, no strong modes are observed near 980 cm^{-1} in the RR spectrum of the 13-demethyl rhodopsin (Figure 6C). The 11-*cis* PSB chromophore in rhodopsin, on the other hand, has a twisted polyene backbone, and its point group may be approximated as C_2 . In the RR spectrum of rhodopsin, the strong intensity of its $C_{11}=C_{12}$ HOOP mode (Figure 3) is consistent with the idea that lowering of the molecular symmetry relaxes restrictions on the RR scattering of " A_2 " modes. A similar enhancement of mode intensity is expected for off-resonance or preresonance excitation. The $C_{11}=C_{12}$ HOOP is strong in the off-resonance spectrum of the 11-*cis* PSB and rhodopsin, but weak in the spectrum of the 13-demethyl PSB. In contrast to A_2 -like modes, resonance Raman scattering by B_1 modes will remain symmetry-forbidden in C_2 . Consistent with this prediction, there is no strong line between 740 and 760 cm^{-1} that can be assigned to a $C_{11}=C_{12}$ HOOP mode of B (or B_1) symmetry in the rhodopsin RR spectrum.⁷³

The RR spectrum of 9-demethyl rhodopsin may be used as a control in our identification of A_2 normal modes. The absence of the 9-methyl group does not change the geometry of the polyene from that of the 11-*cis* PSB, so its molecular point group would still be approximately C_2 . Therefore, a HOOP mode with predominantly $C_{11}=C_{12}$ A_2 HOOP character is expected to retain its strong RR activity in 9-demethyl rhodopsin. Inspection of its RR spectrum and the comparison with that of 13-demethyl rhodopsin show that, indeed, the 9-demethyl rhodopsin exhibits strong HOOP intensity at 993 cm^{-1} .

The intensities of other pseudo A_2 normal modes, in principle, will show similar enhancements when the point group changes from C_{2v} to C_2 . In particular, the RR activity of the $C_{11}=C_{12}$ torsional mode should parallel that of the $C_{11}=C_{12}$ HOOP mode; the torsion intensity will be zero or very weak in 13-demethyl rhodopsin and strong in rhodopsin. Comparing the low-frequency regions of the two pigment spectra (Figure 7A and D), we see that the modes at 568 and 260 cm^{-1} acquire intensity in rhodopsin just as observed for the 970-cm^{-1} HOOP mode. On the basis of the similarity of their Raman activities, the symmetries of the 260- and 568-cm^{-1} modes are assigned as A_2 -like or A species.

The Raman activities of the remaining low-frequency modes at 93, 131, 246, 320, and 446 cm^{-1} do not conform to the behavior exhibited by the modes at 260, 568, and 970 cm^{-1} . Similar Raman-active modes are detected in 13-demethyl rhodopsin at ~ 92 , 128, 245, 328, and 440 cm^{-1} , albeit with slightly altered intensities and/or shifted frequencies. The fact that these modes display RR-intensity or "A"-term scattering activity in rhodopsin, and, more importantly, also in 13-demethyl rhodopsin, suggests naively that their symmetry labels may be " A_1 ". However, the designation of a symmetry label as in-plane or out-of-plane for these modes cannot be deduced using the same criteria applied to the 260- and 568-cm^{-1} modes, because that depended on correlating intrinsic structural differences between 11-*cis* PSB and its 13-demethyl analogue to the differences in the Raman activities of certain normal modes. In

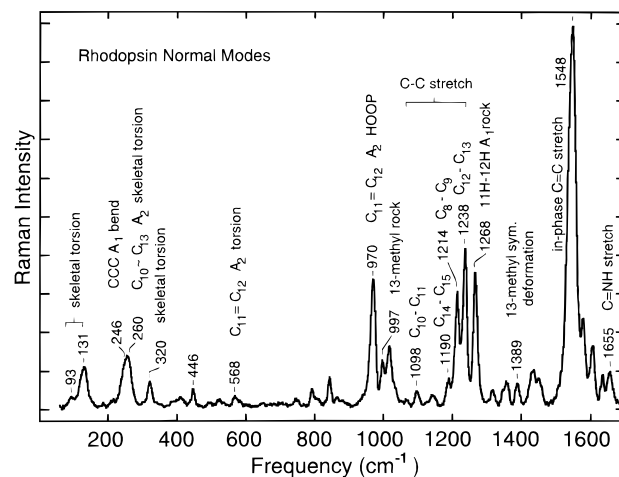


Figure 13. Resonance Raman spectrum of rhodopsin summarizing the normal mode assignments of fundamental transitions between 50 and 1700 cm^{-1} .

this case, none of the modes, except for the one at 246 cm^{-1} , exhibit intensity in the model compound spectra (Figure 9). The 11-*cis* PSB modes at 93, 131, 320, and 446 cm^{-1} have intrinsically weak Raman activity in solution spectra, but their activities increase significantly in the protein. This change is most likely a result of specific protein-induced perturbations of the structure and/or geometry of the chromophore in the asymmetric binding pocket. If the perturbation is localized to a particular region of the polyene, then it will displace only a subset of the normal mode coordinates and alter their equilibrium positions. Accordingly, the relative Raman scattering strengths of these affected modes will be different in the protein. In-plane pseudo- A_1 modes are generally Raman-active in both the solution and pigment spectra, but their intensities may exhibit some environmental sensitivity (Figures 9 and 10). On the other hand, an abrupt increase in Raman scattering strength is more consistent with a change in the activity of an out-of-plane (i.e. pseudo- A_2) mode that becomes Raman-allowed due to distortions introduced in the polyene structure. The $C_7=C_8$ HOOP mode of isorhodopsin at $\sim 960\text{ cm}^{-1}$ is an example of an out-of-plane mode that experiences this kind of change. The Raman activities of the rhodopsin modes at 93, 131, 320, and 446 cm^{-1} also fit this expected pattern for out-of-plane vibrations, and therefore their symmetry species are assigned as " A_2 ". The existence of analogous modes in 13-demethyl rhodopsin suggests that the protein may perturb the structures of the native 11-*cis* chromophore and its 13-demethyl analogue in a similar way. Slight differences in the relative intensities of the 328- and 440-cm^{-1} modes in 13-demethyl rhodopsin compared to those of the 320- and 446-cm^{-1} modes in rhodopsin may be explained as due to subtle variations in the degree of distortions of the two chromophores.

The 246-cm^{-1} mode in rhodopsin is consistently assigned as an in-plane A_1 vibration because it has RR activity in 13-demethyl rhodopsin. Moreover, this mode apparently correlates with the 11-*cis* PSB mode at 236 cm^{-1} , and an analogous 246-cm^{-1} mode in 13-demethyl rhodopsin is also Raman-active in its PSB model compound. The Raman activity of the 246-cm^{-1} mode in both model compounds further supports the description of its symmetry species as totally symmetric.

Normal Mode Assignments. Figure 13 summarizes the vibrational assignments of the fundamental modes detected in the resonance Raman spectrum of rhodopsin. The mode at 568 cm^{-1} is assigned as the $C_{11}=C_{12}$ torsion of the 11-*cis* retinal PSB chromophore in rhodopsin. This frequency is closest to

that calculated for the $C_{11}=C_{12}$ torsion mode (543 cm^{-1}) in the 11-*cis* PSB, and it is the only mode whose observed isotopic frequency pattern resembles the calculated pattern. Consistent with this assignment, the symmetry of the 568-cm^{-1} mode is A_2 . The frequency of this torsion in the 11-*cis* PSB molecule is close to the torsional frequency of the central ethylenic bond in *cis*-stilbene which has been assigned at 560 cm^{-1} .⁶³ *cis*-Stilbene has been utilized as a model system for studying photoisomerization in polyenes. The similarity of the two frequencies suggests that a localized $C=C$ torsional mode at $\sim 560\text{ cm}^{-1}$ may be a characteristic of a sterically hindered *cis* double bond in polyenes.

The Raman activity pattern of the 260-cm^{-1} mode is consistent with that of a torsional mode of A_2 symmetry, and the isotopic data indicate that this mode involves motion of atoms between C_{10} and C_{13} . We cannot directly correlate it to one of the calculated modes of the 11-*cis* PSB, but it is closest in frequency to the calculated modes at 228, 242, and 282 cm^{-1} , which may generally be described as delocalized skeletal twists. Therefore, the 260-cm^{-1} mode of rhodopsin most likely represents a skeletal twisting vibration which includes torsion along the $C_{10}-C_{11}$ and/or $C_{12}-C_{13}$ bond. The contribution of other vibrational coordinates to this mode cannot be specified in the absence of additional isotopic derivative data.

The mode at 246 cm^{-1} is assigned to an in-plane in-phase CCC bend because its symmetry species is A_1 . The sensitivity of this mode to ^{13}C substitution of the $C_{12}-C_{13}$ bond and to deuteration at C_{11} and C_{12} indicates that various CCC bend coordinates which include C_{11} , C_{12} , and C_{13} atoms contribute to the normal mode vibration. Such a low frequency for an in-phase A_1 CCC bending mode is not unusual since CCC bending modes in *cis*-hexatriene are found as low as $\sim 177\text{ cm}^{-1}$.⁷⁴ Furthermore, this is the only low-frequency mode that has Raman activity in both rhodopsin and 13-demethyl rhodopsin and their respective PSB model compounds. An analogous mode is also present in 9-demethyl rhodopsin. The fact that this mode exists in all 11-*cis* retinals suggests that it is a characteristic vibration of a polyene with a 11-*cis* configuration.

The remaining low-frequency modes (93 , 131 , 320 , and 446 cm^{-1}) are assigned as A_2 torsional vibrations that acquire Raman activity because of protein-induced distortion of the retinal geometry. The modes at 93 , 131 , and 320 cm^{-1} , in particular, are observed in all four pigments (i.e. all rhodopsins and isorhodopsin), but not in their respective model compounds. This pattern is consistent with the notion that activity in these modes is turned on by the interaction of retinal with the asymmetric protein binding pocket. Moreover, the similarity of the frequencies and the relative intensities of these modes in the different pigments suggest that they reflect distortions that are common to both 11-*cis* and 9-*cis* chromophores. The energy-minimized structures of the two retinal isomers are similar at the ionone ring and between C_6 and C_9 , and the normal mode analysis predicts several modes with C_6-C_7 and C_8-C_9 single bond torsional character below 200 cm^{-1} in the 11-*cis* PSB as well as in the 9-*cis* PSB. Therefore, the intensity in these modes may represent torsional activity along $C-C$ bonds between C_6 and C_9 .

Excited-State Isomerization of Rhodopsin. The initial nuclear dynamics of the photochemically excited 11-*cis* chromophore in rhodopsin are dictated by the slopes of the excited-state potential energy surface along the various normal coordinates.^{25,26} When separable harmonic surfaces are used to model the multidimensional electronic surfaces, the excited-state slope along a normal coordinate j evaluated at the ground-

state equilibrium geometry is equal to $h\nu_j\Delta_j$, where Δ_j is the dimensionless displacement between the minima of the ground- and excited-state harmonic wells with frequencies ν_j . The geometry change along a internal coordinate δ_i , in turn, is proportional to the weighted sum of the Δ_j 's and coefficients A_j 's of all normal coordinates that project onto this internal coordinate: $\sum_j A_j w_j^{-1/2} \Delta_j$. Since RR intensity is roughly proportional to Δ^2 , the intensities in the RR spectrum provide a direct mode-specific measure of the extent of excited-state nuclear distortions that take place after electronic excitation. The quantitative modeling of the absolute intensities also places constraints on the amount of electronic homogeneous and inhomogeneous broadening. The analysis of the RR intensities, therefore, provides detailed information about the early excited-state processes that are pertinent for discriminating between theoretical models^{3,15,75} of the *cis-trans* isomerization in rhodopsin and ultimately for understanding the mechanism of this ultrafast and highly efficient reaction.

$C_{11}=C_{12}$ Torsional Dynamics. The isomerization of the 11-*cis* PSB chromophore in rhodopsin is complete in $\sim 200\text{ fs}$.^{13,14} This short time for the formation of the ground-state photo-product implies that the departure of the excited molecular state out of the FC region occurs on a time scale of $<100\text{ fs}$, consistent with measurements of the fluorescence lifetime that indicate a T_1 time of $\sim 50\text{ fs}$.^{8,9} It has been proposed that this ultrafast isomerization is driven by the instantaneous relaxation of the excited polyene via torsional modes that project directly along the $C_{11}=C_{12}$ torsion. These dynamics may be realized by steep slopes on the FC region of the S_1 energy surface along relevant torsional coordinates.

Our finding that fundamental transitions of $C_{11}=C_{12}$ torsional modes at 260 and 568 cm^{-1} are RR active gives direct experimental support for this idea. The displacements of the low-frequency modes quantitated from the most recent RR intensity analysis are listed in Table 1.⁷⁶ The Δ along the 568-cm^{-1} mode indicates that the retinal chromophore on the S_1 surface instantaneously experiences a torque that twists the molecule about the $C_{11}=C_{12}$ bond. This initial rotation is accompanied by skeletal distortion, represented by the displacement of the 260-cm^{-1} mode, resulting from concerted A_2 torsions about other $C-C$ and $C=C$ bonds. The slopes along the 260 - and 568-cm^{-1} coordinates accelerate and help guide the nuclei toward isomerization about the $C_{11}=C_{12}$ bond. Consistent with this interpretation, the isomerization rates of isorhodopsin and 13-demethyl rhodopsin, which lack RR activity in the relevant torsional coordinates, are a factor of 3 and 2, respectively, slower than that of rhodopsin.^{22,23} The importance of initial excited-state displacements to the overall photochemistry has also been suggested for the conrotatory ring-opening dynamics of cyclohexadiene^{27,77} and the isomerization of *cis*-stilbene.^{63,78}

The relaxation of the excited chromophore on the S_1 surface involves additional skeletal deformations that are represented by displacements along the 93 -, 131 -, 320 -, and 246-cm^{-1} modes. Motion due to the 93 -, 131 -, and 320-cm^{-1} modes probably correspond to torsions of coordinates closer to the ring and between C_6 and C_9 . CCC bending activity along the 246-cm^{-1} mode is specific to the 11-*cis* retinal analogues and may reflect the mixing of bend and torsion coordinates that occur during large out-of-plane deformation of polyene geometry.

B-Term Raman Activity of Torsional Modes. Although the Δ s of the low-frequency modes contribute to the Condon-based Gaussian broadening of the absorption spectrum, additional phenomenological damping is still required, even at 1.5

K, to model the diffuseness of the rhodopsin absorption spectrum.^{10–12} There are at least two likely explanations for the physical origin of this damping. One explanation is that it arises from the decrease of the S_0 – S_1 transition moment during twisting of the $C_{11}=C_{12}$ bond,¹² which mixes the zero-order S_1 and the S_2 electronic states. If this mechanism was operating, the Raman-scattering cross-sections of nontotally symmetric normal coordinates that vibronically couple the two states would display B-term enhancement.⁷² Second, the damping may represent dielectric relaxation resulting from the coupling between the protein dielectric environment and the large excited-state dipole of the 11-*cis* chromophore.^{79,80}

Normal modes with pseudo- A_1 symmetry, such as the in-phase C=C stretch at 1548 cm^{-1} and the fingerprint C–C stretching modes, scatter predominantly via only the A-term mechanism, and the fractional contribution to the total Raman scattering intensity by these A-term enhanced modes stays approximately constant as a function of excitation wavelength (Figure 11). Away from the resonance, the effective contribution to the Raman scattering from higher order terms in the polarizability expansion becomes greater or comparable to the A-term scattering.^{24,71} As a result, modes with the correct symmetry to vibronically couple electronic surfaces via one of the higher order processes will display increased scattering intensity compared to modes that scatter only via the A-term process.⁷² We observe comparatively stronger Raman scattering by the 568- and 260- cm^{-1} modes with preresonant excitation, which are consistent with B-term enhancement of their intensities. These torsional modes display a ~ 2 -fold increase in their relative intensities when excited with 792 nm compared to the intensity obtained with resonant 488-nm excitation.

Semiempirical electronic structure calculations on model PSB polyene systems show that C=C twists mix the zero-order polyene S_1 and S_2 states, i.e., the low-lying B_2 and the second-excited A_1 states.^{81,82} This means that the vibronic coupling matrix element $\langle S_1 | \partial/\partial Q_a | S_2 \rangle$,²⁴ where Q_a is a coupling normal coordinate, is nonzero. Rotation about the $C_{11}=C_{12}$ bond, in particular, causes the strongest state mixing and produces a barrierless S_1 surface and a minimal S_0 – S_1 energy gap at the 90°-twisted geometry.⁸¹ Since B-term scattering is proportional to the matrix element $\langle S_1 | \partial H / \partial Q_a | S_2 \rangle$, the $C_{11}=C_{12}$ torsion mode and other skeletal torsional modes are expected to show stronger Raman scattering off-resonance.⁸³ The observed increase in Raman scattering by the 568- and 260- cm^{-1} modes is consistent with these theoretical predictions. *The B-term enhancements of the 568- and 260- cm^{-1} Raman intensities provide direct spectroscopic evidence for the torsional mixing of S_1 and S_2 surfaces during the early dynamics of the isomerization.* These data are also consistent with the idea that coordinate-dependent decay of the transition moment contributes to the phenomenological damping term.

Trajectory of Nuclear Dynamics on the S_1 Surface. The vibrational assignments of the torsional modes and the analysis of the Raman scattering intensities presented here enable us to develop a qualitative mode-specific picture of the early nuclear isomerization dynamics of the 11-*cis* retinal chromophore in rhodopsin and to understand the causal relationship between the FC dynamics and the isomerization mechanism. Photoexcitation of the chromophore to the S_1 surface results in a reduction of C=C bond order, which is greatest at the $C_{11}=C_{12}$ bond.⁸¹ This causes torsional relaxation along three primary out-of-plane normal coordinates. The dynamics first proceeds along the high-frequency $C_{11}=C_{12}$ A_2 HOOP coordinate in which the 11 and 12 hydrogens move out of the local plane in

opposite directions. This motion reflects the initiation of the pyramidalization of C_{11} and C_{12} centers.³¹ The displacements of hydrogen atoms are followed by rotation of the $C_{11}=C_{12}$ bond along the 568- cm^{-1} coordinate, which displaces C_{10} and C_{13} atoms. The change in the $C_{11}=C_{12}$ dihedral angle also progressively mixes more of the doubly excited A_1 electronic character into the pseudo- B_2 S_1 state to generate a barrierless S_1 trajectory. As the local distortion between C_{10} and C_{13} develops, the chromophore begins to undergo skeletal deformation along the 260- cm^{-1} normal coordinate. This deformation proceeding on a slower time scale probably represents partial rotations of several C–C and C=C bonds, including the C_{10} – C_{11} and C_{12} – C_{13} torsion coordinates. The large Δ of this mode indicates that the 260- cm^{-1} distortion is a dominant channel for torsional relaxation in the early part of the isomerization trajectory. Simulation of retinal isomerization within the constraint of a solvent cavity optimized for the 11-*cis* chromophore shows that partial rotations are necessary if the overall motion along the $C_{11}=C_{12}$ isomerization coordinate is to follow a path of minimum energy on S_1 .⁵⁴ In addition, partial rotations enhance the coupling of the S_1 and S_0 surfaces at the 90°-twisted transition state.⁸¹ Taken together, the conclusions from these electronic structure calculations suggest that the dynamics along the 260- cm^{-1} coordinate serve dual purposes. First, the resulting partial rotations reduce the volume swept out during *cis*–*trans* isomerization and, thereby, minimize kinetic-energy loss due to excessive collision of the retinal with the protein. Second, this dynamics maximizes the transition probability from the S_1 to S_0 surface as the $C_{11}=C_{12}$ bond twists.

Role of Opsin in Isomerization. The displacements of the $C_{11}=C_{12}$ torsional coordinates are associated with the intrinsic ground-state distortion of the 11-*cis* geometry between C_{10} and C_{13} , caused by steric hindrance between the 10H and the 13-methyl group. In the planar 13-demethyl analogue chromophore, reductions of the $C_{11}=C_{12}$ torsional and HOOP RR intensities are observed (Figures 3A and 6C) and are correlated with slower isomerization speed and lower quantum yield.²³ The restoration of the steric interaction by attaching a methyl group to C_{10} as in the 10-methyl 13-demethyl retinal analogue restores the RR intensities.²¹ These results support the suggestion that the nonbonded interaction between 10H and 13-methyl plays a role in driving the early isomerization dynamics. However, this interaction alone is not sufficient to explain the observed torsional Δ s and the resulting ultrafast photochemistry of the chromophore because the isomerization¹⁹ of the 11-*cis* retinal PSB *n*-butylamine in methanol, although very fast, is still approximately an order of magnitude slower than in rhodopsin, and its excited-state Δ s for the $C_{11}=C_{12}$ torsional coordinates, inferred from the low RR intensity of the $C_{11}=C_{12}$ HOOP mode, are smaller.³³ We have earlier shown that the HOOP intensity is directly correlated to the intensities of the 260- and 568- cm^{-1} modes (vide supra).

The protein environment could influence the isomerization rate and yield by modifying the electronic structure of retinal PSB via electrostatic or hydrogen-bonding interactions and/or by displacing the S_0 – S_1 surfaces along key normal coordinates through distortion of retinal geometry via steric interactions. Contribution from the latter effect is suggested from the comparison of the preresonance spectra of the 11-*cis* PSB model compound and rhodopsin (Figures 9 and 10). The relative intensities of modes at 260, 568, and 970 cm^{-1} are higher in rhodopsin. Since the preresonance intensities more accurately reflect the lower symmetry of the ground-state molecular structure, the observed increases are consistent with the idea

that the asymmetric opsin binding pocket adds distortion between C₁₀ and C₁₃, which results in specific displacements along the relevant C₁₁=C₁₂ torsional coordinates. This opsin–retinal interaction is mediated by the 13-methyl group because its removal abolishes the twist of the polyene. However, it also requires a native retinal structure since we find that the removal of the 9-methyl group affects the torsional dynamics. In the 9-demethyl rhodopsin, the Δ of the C₁₁=C₁₂ torsion coordinate (at 571 cm⁻¹) is increased, while the Δ of the 260-cm⁻¹ skeletal mode is reduced (Figure 6B). The resultant alteration in the initial dynamics may explain the perturbed photochemistry of 9-demethyl rhodopsin.⁴⁹

The isomerization quantum yields of all retinal chromophores (9-*cis*, 11-*cis*, and 13-demethyl 11-*cis*) are consistently (2–3-fold) higher inside the opsin than in solution,⁸⁴ indicating that the opsin facilitates the reaction by a common general mechanism. In this regard, it is noteworthy that the binding of retinals and analogues to the opsin is correlated with increases in the RR intensities of the modes at ~95, 135, and 320 cm⁻¹, presumably due to torsional distortions near the ionone ring. Excited-state activity along these coordinates may play a role in the isomerization mechanism in all retinals.

On the whole, the analysis of the torsional intensities suggests that the protein cavity facilitates isomerization of retinal by solvating the chromophore in a way that focuses excited-state nuclear motion along coordinates that project on the reaction coordinate. The protein restraints, most likely steric in nature, minimize dephasing of the excited molecule and prevent it from distorting along dissipative torsional and bending modes.

Tunneling Dynamics. The excited-state isomerization dynamics of the 11-*cis* PSB chromophore in rhodopsin goes beyond the traditional picture of photochemical isomerization in which excited-state relaxation and equilibration are followed by partitioning of the excited molecule to the *cis* or *trans* ground-state photoproduct via a common ~90°-twisted transition state.⁸⁵ The vibrationally coherent and extremely rapid isomerization is instead more appropriately modeled by a dynamic tunneling mechanism that predicts a direct correlation between the quantum yield and the velocity of the isomerization dynamics along the reactive coordinate.^{86,87} The transition probability in a simple one-dimensional Landau–Zener model of this process is proportional to $\exp[-(\Delta E)^2/(2\hbar|\Delta F|\mathbf{v})]$, where ΔE and ΔF are the energy gap and the slope difference, respectively, between the S₀ and S₁ surfaces, and \mathbf{v} is the nuclear velocity along the torsional isomerization coordinate. This formula suggests that the crossing probability, and, hence, the quantum yield, can be optimized by enhancing the initial C₁₁=C₁₂ torsional dynamics.

Ultrafast dynamics along the reactive C₁₁=C₁₂ torsion coordinate are realized by protein-induced displacement of the S₀ and S₁ FC surfaces along the 568-cm⁻¹ coordinate, which ensures that kinetic energy is instantaneously funneled into rotation of this bond. The resulting mixing of the S₁ and S₂ states, which becomes greater as the dihedral angle approaches 90°, produces a barrierless trajectory on the nonadiabatic S₁ surface which accelerates the nuclear dynamics along the reactive coordinate. In addition, partial distortion of the skeletal geometry, represented by motion along the 260-cm⁻¹ mode, brings the molecule into a region of stronger S₀–S₁ coupling by minimizing ΔE and simultaneously maximizing ΔF between these surfaces. The dynamics along the two coordinates enable the isomerization to occur at a rate that is much faster compared to the time scale of vibrational dephasing or other excited-state decay processes.

The high quantum yield of the isomerization in rhodopsin is a consequence of the faster dynamics and the unique characteristics of the electronic-state mixing caused by twisting of the C₁₁=C₁₂ bond. It follows that the lower yields in isorhodopsin and 13-demethyl rhodopsin are most likely due to the absence of torsional Δ s which directly project along their respective isomerization coordinates (vide supra), thus, resulting in slower initial dynamics.^{15,21,22} In isorhodopsin, an energy barrier to rotation about the C₉=C₁₀ bond on the S₁ surface⁸¹ further slows the dynamics, leading to the dissipation of kinetic energy through competing relaxation channels.

Coherent Vibrations in Bathorhodopsin. The RR spectrum of bathorhodopsin presented here reveals many Raman-active low-frequency modes. We assign most of these modes to C–C and C=C torsional coordinates of the all-*trans* chromophore, in analogy with the assignments in rhodopsin. These torsional Raman activities provide additional evidence that the backbone geometry of the chromophore in bathorhodopsin is distorted^{31,42} and lend further support to the idea that ~30 kcal/mol of the absorbed photon energy⁸⁸ is stored primarily in the conformational distortion of the chromophore.^{42,89}

The Fourier power spectrum of the oscillatory femtosecond kinetic traces of bathorhodopsin absorption contains several frequency components at approximately 60, 100, 125, 190, 210, 260, and 270 cm⁻¹, with the 60-cm⁻¹ vibration being the most dominant.¹⁵ The presence of these oscillations indicates that the impulsively produced all-*trans* photoproduct is executing coherent skeletal vibration in the ground state. Several Raman-active modes (~54, 119, 128, 151, 204, 262, 276, 324, and 376 cm⁻¹) are detected in the bathorhodopsin spectrum (Figure 8) at about the same frequencies as the vibrational modes recovered from the Fourier deconvolution. The much lower intensity of the ~60-cm⁻¹ mode in the RR spectrum compared to that in the power spectrum is explained by the fact that its RR intensity is dampened by multimode effects and other fast excited-state dephasing and decay processes. For example, the 93-cm⁻¹ mode in rhodopsin which has a relative intensity similar to that of the 54-cm⁻¹ mode in bathorhodopsin, has a Δ of 0.90. The observation of these RR-active low-frequency modes in bathorhodopsin supports the earlier assignment of the oscillations in the femtosecond data to coherent motion of the chromophore in the *ground state* of the photoproduct.

Conclusion

We have assigned the C₁₁=C₁₂ torsional mode of rhodopsin at 568 cm⁻¹. In addition, the strong RR band at 260 cm⁻¹ has been assigned to a “A₂” skeletal distortion of coordinates between C₁₀ and C₁₃. An explicit picture of the femtosecond excited-state dynamics based on resonance Raman intensities is presented in a forthcoming paper.⁷⁶

Acknowledgment. We thank Linda Peteanu for assistance with measurements of the rhodopsin spectra in the early part of this work, David Wexler for performing the thermalized resonance Raman intensity calculation, and Daniel Chiu, May Chan, and Ivan El-Sayed for assistance with rhodopsin preparation. We also thank David Wexler and Gerd Kochendoerfer for helpful discussions. This work was supported by grants from the National Institutes of Health (EY 02051) and by the National Science Foundation (CHE 94-19714) to R.A.M. P.V. acknowledges generous support from the European Community Biotechnology Program CEC Project PL 92-0467.

References and Notes

- (1) Yoshizawa, T.; Wald, G. *Nature* **1963**, *197*, 1279. For reviews, see: (a) Birge, R. R. *Biochim. Biophys. Acta* **1990**, *1016*, 293. (b) Kochendoerfer, G. G.; Mathies, R. A. *Israel J. Chem.* **1995**, *35*, 211.
- (2) (a) Nathans, J. *Biochemistry* **1992**, *31*, 4923. (b) Sakmar, T. P.; Fahmy, K. *Israel J. Chem.* **1995**, *35*, 325.
- (3) Tallent, J. R.; Hyde, E. W.; Findsen, L. A.; Fox, G. C.; Birge, R. R. *J. Am. Chem. Soc.* **1992**, *114*, 1581.
- (4) (a) Busch, G. E.; Applebury, M. L.; Lamola, A. A.; Rentzepis, P. M. *Proc. Natl. Acad. Sci. U.S.A.* **1972**, *69*, 2802. (b) Spalink, J. D.; Reynolds, A. H.; Rentzepis, P. M.; Sperling, W.; Applebury, M. L. *Proc. Natl. Acad. Sci. U.S.A.* **1983**, *80*, 1887.
- (5) Monger, T. G.; Alfano, R. R.; Callender, R. H. *Biophys. J.* **1979**, *27*, 105.
- (6) Hayward, G.; Carlsen, W.; Siegman, A.; Stryer, L. *Science* **1981**, *211*, 942.
- (7) Kandori, H.; Shichida, Y.; Yoshizawa, T. *Biophys. J.* **1989**, *56*, 453.
- (8) Doukas, A. G.; Junnarkar, M. R.; Alfano, R. R.; Callender, R. H.; Kakitani, T.; Honig, B. *Proc. Natl. Acad. Sci. U.S.A.* **1984**, *81*, 4790.
- (9) Kochendoerfer, G. G.; Mathies, R. A. *J. Phys. Chem.* **1996**, *100*, 14526.
- (10) Loppnow, G. R.; Mathies, R. A. *Biophys. J.* **1988**, *54*, 35.
- (11) Shreve, A. P.; Mathies, R. A. *J. Phys. Chem.* **1995**, *99*, 7285.
- (12) Loppnow, G. R.; Mathies, R. A.; Middendorf, T. R.; Gottfried, D. S.; Boxer, S. G. *J. Phys. Chem.* **1992**, *96*, 737.
- (13) Schoenlein, R. W.; Peteanu, L. A.; Mathies, R. A.; Shank, C. V. *Science* **1991**, *254*, 412.
- (14) Peteanu, L. A.; Schoenlein, R. W.; Wang, Q.; Mathies, R. A.; Shank, C. V. *Proc. Natl. Acad. Sci. U.S.A.* **1993**, *90*, 11762.
- (15) Wang, Q.; Schoenlein, R. W.; Peteanu, L. A.; Mathies, R. A.; Shank, C. V. *Science* **1994**, *266*, 422.
- (16) Becker, R. S. *Photochem. Photobiol.* **1988**, *48*, 369.
- (17) Koyama, Y.; Kubo, K.; Komori, M.; Yasuda, H.; Mukai, Y. *Photochem. Photobiol.* **1991**, *54*, 433.
- (18) Huppert, D.; Rentzepis, P. M. *J. Phys. Chem.* **1986**, *90*, 2813.
- (19) Kandori, H.; Katsuta, Y.; Ito, M.; Sasabe, H. *J. Am. Chem. Soc.* **1995**, *117*, 2669.
- (20) Warshel, A.; Karplus, M. *J. Am. Chem. Soc.* **1974**, *96*, 5677.
- (21) Kochendoerfer, G. G.; Verdegem, P. J. E.; van der Hoef, I.; Lugtenburg, J.; Mathies, R. A. *Biochemistry* **1996**, *35*, 16230.
- (22) Schoenlein, R. W.; Peteanu, L. A.; Wang, Q.; Mathies, R. A.; Shank, C. V. *J. Phys. Chem.* **1993**, *97*, 12087.
- (23) Wang, Q.; Kochendoerfer, G. G.; Schoenlein, R. W.; Verdegem, P. J. E.; Lugtenburg, J.; Mathies, R. A.; Shank, C. V. *J. Phys. Chem.* **1996**, *100*, 17388.
- (24) Tang, J.; Albrecht, A. C. In *Raman Spectroscopy*; Szymanski, H. A., Ed.; Plenum: New York, 1970; Vol. 2, p 33.
- (25) Lee, S.-Y.; Heller, E. J. *J. Chem. Phys.* **1979**, *71*, 4777.
- (26) Myers, A. B.; Mathies, R. A. In *Biological Applications of Raman Spectroscopy: Resonance Raman Spectra of Polyenes and Aromatics*; Spiro, T. G., Ed.; Wiley: 1987; Vol. 2, p 1.
- (27) (a) Reid, P. J.; Lawless, M. K.; Wickham, S. D.; Mathies, R. A. *J. Phys. Chem.* **1994**, *98*, 5597. (b) Lawless, M. K.; Wickham, S. D.; Mathies, R. A. *Acc. Chem. Res.* **1995**, *28*, 493.
- (28) Mathies, R.; Oseroff, A. R.; Stryer, L. *Proc. Natl. Acad. Sci. U.S.A.* **1976**, *73*, 1.
- (29) Mathies, R.; Freedman, T. B.; Stryer, L. *J. Mol. Biol.* **1977**, *109*, 367.
- (30) Callender, R. H.; Doukas, A.; Crouch, R.; Nakanishi, K. *Biochemistry* **1976**, *15*, 1621.
- (31) Eyring, G.; Curry, B.; Broek, A.; Lugtenburg, J.; Mathies, R. *Biochemistry* **1982**, *21*, 384.
- (32) Mathies, R. A.; Smith, S. O.; Palings, I. In *Biological Applications of Raman Spectroscopy*; Spiro, T. G., Ed.; Wiley: New York, 1987; Vol. 2, p 59.
- (33) Palings, I.; Pardo, J. A.; van den Berg, E.; Winkel, C.; Lugtenburg, J.; Mathies, R. A. *Biochemistry* **1987**, *26*, 2544.
- (34) Groesbeek, M.; Rood, G. A.; Lugtenburg, J. *Recl. Trav. Chim. Pays-Bas* **1992**, *111*, 149.
- (35) Broek, A. D.; Lugtenburg, J. *Recl. Trav. Chim. Pays-Bas* **1980**, *99*, 363.
- (36) Broek, A. D.; Muradin-Szweykowska, M.; Courtin, J. M. L.; Lugtenburg, J. *Recl. Trav. Chim. Pays-Bas* **1983**, *102*, 46.
- (37) Mathies, R. *Methods Enzymol.* **1982**, *88*, 633.
- (38) Oseroff, A. R.; Callender, R. H. *Biochemistry* **1974**, *13*, 4243.
- (39) Mathies, R.; Yu, N. *J. Raman Spectrosc.* **1978**, *7*, 349.
- (40) Miller, F. A.; Harney, B. M. *Appl. Spectrosc.* **1970**, *24*, 291.
- (41) Warshel, A.; Deakyne, C. *Chem. Phys. Lett.* **1978**, *53*, 459.
- (42) Palings, I.; van den Berg, E. M. M.; Lugtenburg, J.; Mathies, R. A. *Biochemistry* **1989**, *28*, 1498.
- (43) Curry, B.; Palings, I.; Broek, A. D.; Pardo, J. A.; Lugtenburg, J.; Mathies, R. *Adv. Infrared Raman Spectrosc.* **1985**, *12*, 115.
- (44) Blatz, P. E.; Lin, M.; Balasubramanian, P.; Balasubramanian, V.; Dewhurst, P. B. *J. Am. Chem. Soc.* **1969**, *91*, 5930.
- (45) Kropf, A.; Whittenberger, B. P.; Goff, S. P.; Waggoner, A. S. *Exp. Eye Res.* **1973**, *17*, 591.
- (46) Doukas, A. G.; Aton, B.; Callender, R. H.; Ebrey, T. G. *Biochemistry* **1978**, *17*, 2430.
- (47) Lin, S. W.; Imamoto, Y.; Fukada, Y.; Shichida, Y.; Yoshizawa, T.; Mathies, R. A. *Biochemistry* **1994**, *33*, 2151.
- (48) Curry, B. U. Ph.D. Dissertation Thesis, University of California at Berkeley, 1983.
- (49) Ganter, U. M.; Schmid, E. D.; Perez-Sala, D.; Rando, R. R.; Siebert, F. *Biochemistry* **1989**, *28*, 5954.
- (50) Siebert, F.; Mantele, W.; Gerwert, K. *Eur. J. Biochem.* **1983**, *136*, 119.
- (51) Bagley, K. A.; Balogh-Nair, V.; Croteau, A. A.; Dollinger, G.; Ebrey, T. G.; Eisenstein, L.; Hong, M. K.; Nakanishi, K.; Vittitow, J. *Biochemistry* **1985**, *24*, 6055.
- (52) Nelson, R.; de Riel, J. K.; Kropf, A. *Proc. Natl. Acad. Sci. U.S.A.* **1970**, *66*, 531.
- (53) Ganter, U. M.; Gartner, W.; Siebert, F. *Eur. Biophys. J.* **1990**, *18*, 295.
- (54) Warshel, A.; Barboy, N. *J. Am. Chem. Soc.* **1982**, *104*, 1469.
- (55) Eyring, G.; Curry, B.; Mathies, R.; Fransen, R.; Palings, I.; Lugtenburg, J. *Biochemistry* **1980**, *19*, 2410.
- (56) Deng, H.; Callender, R. H. *Biochemistry* **1987**, *26*, 7418.
- (57) Birge, R. R.; Sullivan, M. J.; Kohler, B. E. *J. Am. Chem. Soc.* **1976**, *98*, 358.
- (58) Cookingham, R. E.; Lewis, A.; Lemley, A. T. *Biochemistry* **1978**, *17*, 4699.
- (59) Gilardi, R. D.; Karle, I. L.; Karle, J. *Acta Crystallogr.* **1972**, *B28*, 2605.
- (60) Drikos, G.; Rueppel, H.; Dietrich, H.; Sperling, W. *FEBS Lett.* **1981**, *131*, 23.
- (61) Rowan, R., III; Warshel, A.; Sykes, B. D.; Karplus, M. *Biochemistry* **1974**, *13*, 970.
- (62) Warshel, A. *J. Chem. Phys.* **1975**, *62*, 214.
- (63) Myers, A. B.; Mathies, R. A. *J. Chem. Phys.* **1984**, *81*, 1552.
- (64) Levin, I. W.; Pearce, R. A. R.; Harris, W. J. *J. Chem. Phys.* **1973**, *59*, 3048.
- (65) Levin, I. W.; Pearce, R. A. R. *J. Mol. Spectrosc.* **1974**, *49*, 91.
- (66) Gavin, R. M.; Rice, S. A. *J. Chem. Phys.* **1971**, *55*, 2675.
- (67) Panchenko, Y. N.; Pulay, P.; Torok, F. J. *Mol. Struct.* **1976**, *34*, 283.
- (68) Birge, R. R.; Pierce, B. M. *J. Chem. Phys.* **1979**, *70*, 165.
- (69) The electronic states of the 11-*cis* PSB are also described using the symmetry labels of the parent C_{2h} molecule, as A_g or B_u .^{16,68}
- (70) Colthup, N. B.; Daly, L. H.; Wiberley, S. E. *Introduction to Infrared and Raman Spectroscopy*, 3rd ed.; Academic Press: New York, 1990; p 547.
- (71) Warshel, A.; Dauber, P. *J. Chem. Phys.* **1977**, *66*, 5477.
- (72) Albrecht, A. C.; Hutley, M. C. *J. Chem. Phys.* **1971**, *55*, 4438.
- (73) The $C_{11}=C_{12}$ B₁ HOOP mode has been assigned at 762 cm^{-1} in the 11-*cis* retinal⁴³ and is calculated at ~ 740 cm^{-1} for the 13-demethyl 11-*cis* PSB.
- (74) Ci, X.; Myers, A. B. *J. Chem. Phys.* **1992**, *96*, 6433.
- (75) Weiss, R. M.; Warshel, A. *J. Am. Chem. Soc.* **1979**, *101*, 6131.
- (76) Wexler, D.; Mathies, R. A. *J. Phys. Chem.*, submitted for publication.
- (77) Trulson, M. O.; Dollinger, G. D.; Mathies, R. A. *J. Chem. Phys.* **1989**, *90*, 4274.
- (78) Rodier, J.-M.; Myers, A. B. *J. Am. Chem. Soc.* **1993**, *115*, 10791.
- (79) Mathies, R.; Stryer, L. *Proc. Natl. Acad. Sci. U.S.A.* **1976**, *73*, 2169.
- (80) Wexler, D.; Kochendoerfer, G. G.; Mathies, R. A. In *Femtochemistry and Femtobiology: Ultrafast Reaction Dynamics at Atomic Scale Resolution*; Imperial College Press: London, 1998; Vol. 101, in press.
- (81) Dormans, G. J. M.; Groenenboom, G. C.; van Dorst, W. C. A.; Buck, H. M. *J. Am. Chem. Soc.* **1988**, *110*, 1406.
- (82) Birge, R. R.; Hubbard, L. M. *J. Am. Chem. Soc.* **1980**, *102*, 2195.
- (83) Torsion coordinates of A_2 (A) symmetry normally cannot vibronically couple states of B_2 (B) and A_2 (A) symmetry in the C_{2v} (C_2) point group. However, the mixing of pseudo B and A symmetry states by torsion coordinates is possible in retinal and its PSB because their point groups are technically C_1 . The terminal heteroatom (N or O) causes the doubly excited $(\pi\pi^*)^2$ configurational character of the zero-order A_1 state to mix into the zero-order B_2 state.⁸¹ Experimentally, this mixing is reflected in the nonzero dipole moment of the S_1 state in retinals and their PSB salts.⁷⁹ Thus, the reduced in-plane symmetries of the S_1 and S_2 states make it possible for torsional coordinates to couple the two surfaces.

- (84) Becker, R. S.; Freedman, K. *J. Am. Chem. Soc.* **1985**, *107*, 1477.
(85) Rosenfeld, T.; Honig, B.; Ottolenghi, M.; Hurley, J.; Ebrey, T. G. *Pure Appl. Chem.* **1977**, *49*, 341.
(86) Landau, L. D. *Phys. Z. Sowjetunion* **1932**, *2*, 46.
(87) Zener, C. *Proc. R. Soc. London* **1932**, *A137*, 696.
(88) Schick, G. A.; Cooper, T. M.; Holloway, R. A.; Murray, L. P.; Birge, R. R. *Biochemistry* **1987**, *26*, 2556.
(89) (a) Fahmy, K.; Sakmar, T. P. *Biochemistry* **1993**, *32*, 9165. (b) Han, M.; Smith, S. O. *Biochemistry* **1995**, *34*, 1425. (c) Bifone, A.; deGroot, H. J. M.; Buda, F. *J. Phys. Chem. B* **1997**, *101*, 2954.